Paleogene clockwise tectonic rotations in the forearc of central Andes, Antofagasta region, northern Chile

César Arriagada, Pierrick Roperch, Constantino Mpodozis, Guillaume Dupont-Nivet, Peter Cobbold, Annick Chauvin, Joaquin Cortés

Paleogene clockwise tectonic rotations in the forearc of central Andes, Antofagasta region, northern Chile

César Arriagada,[1,2] Pierrick Roperch,[1] Constantino Mpodozis,[3,4]
Guillaume Dupont-Nivet,[5] Peter R. Cobbold,[2] Annick Chauvin,[2] and Joaquin Cortés[3]

Received 24 October 2001; revised 5 May 2002; accepted 20 May 2002; published 21 January 2003.

[1] For the Central Valley of northern Chile (Antofagasta region), a paleomagnetic analysis of data from 108 sites, mainly in Mesozoic and Paleogene volcanic rocks, has yielded stable remanent magnetization directions for 86 sites. From these data, we infer clockwise tectonic rotations of up to 65° within the forearc domain of the central Andes. The apparent relationship between tectonic rotations and structural trends suggests that rotations occurred mainly during the Incaic orogenic event of Eocene–early Oligocene age. A few paleomagnetic results obtained in Neogene rocks do not show evidence of clockwise rotations. Hence the development of the Bolivian orocline during late Neogene time cannot be explained by simple bending of the whole margin. These results demonstrate that tectonic rotations within the forearc and pre-Cordillera are key elements of early Andean deformation, which should be taken into account by kinematic models of mountain building in the central Andes. *INDEX TERMS:* 1525 Geomagnetism and Paleomagnetism: Paleomagnetism applied to tectonics (regional, global); 8110 Tectonophysics: Continental tectonics—general (0905); 8102 Tectonophysics: Continental contractional orogenic belts; 1599 Geomagnetism and Paleomagnetism: General or miscellaneous; 9360 Information Related to Geographic Region: South America; *KEYWORDS:* paleomagnetism, tectonic rotations, central Andes, northern Chile, Paleogene

Citation: Arriagada, C., P. Roperch, C. Mpodozis, G. Dupont-Nivet, P. R. Cobbold, A. Chauvin, and J. Cortés, Paleogene clockwise tectonic rotations in the forearc of central Andes, Antofagasta region, northern Chile, *J. Geophys. Res.*, *108*(B1), 2032, doi:10.1029/2001JB001598, 2003.

1. Introduction

[2] The Bolivian Orocline, or change in trend of the Andes from NW-SE to N-S near 18°S, is one of the most conspicuous large-scale features of the entire Andean chain. The orocline concept was originally formulated by *Carey* [1958] who envisaged counterclockwise rotation of that segment of the Andes between the Arica–Santa Cruz bend and the Huancabamba bend in the north, essentially after formation of an initially straight Andean chain. *Isacks* [1988] indicated that along-strike variations in the width of the Bolivian Altiplano were associated with differential shortening during plateau uplift. According to this model, a slight original curvature of the Andean continental margin was enhanced by differential shortening during Neogene time, implying rotation of both limbs. The expected rotations are of 5°–10° for the southern limb and 10°–15° for the northern limb. This tectonic model was verified by early paleomagnetic results obtained mostly along the forearc [*Heki et al.*, 1984, 1985; *May and Butler*, 1985; see also review by *Beck*, 1988].

[3] During the last decade numerous new paleomagnetic data have been obtained. They demonstrate that vertical axis rotations are important components of deformation in the central Andes [*Macedo Sanchez et al.*, 1992; *Butler et al.*, 1995; *MacFadden et al.*, 1995; *Randall and Taylor*, 1996; *Randall et al.*, 2001; *Aubry et al.*, 1996; *Somoza et al.*, 1999; *Coutand et al.*, 1999; *Roperch et al.*, 2000; *Arriagada et al.*, 2000; *Somoza and Tomlinson*, 2002]. Most of the new paleomagnetic studies indicate variable amounts of rotation whose magnitudes often exceed those predicted by oroclinal bending associated with uplift of the Altiplano–Puna plateau (see also review by *Beck* [1998]). In situ block rotations, in response to oblique convergence [*Beck*, 1987] and tectonic shortening [*Coutand et al.*, 1999; *Roperch et al.*, 2000], are thus needed to explain the observed spatial variability in the magnitude of rotations.

[4] The suggested relation between plateau uplift and oroclinal bending [*Isacks*, 1988] implies that most of the rotations should have occurred during Neogene time. For the Altiplano–Puna plateau, a good correlation exists between Plateau uplift, deformation and tectonic rotations [*Coutand et al.*, 1999; *Roperch et al.*, 2000]. Within the forearc and the pre-Cordillera of northern Chile (Domeyko Cordillera, Figure 1), the situation is different. There, large rotations are observed in Paleocene rocks [*Hartley et al.*, 1992; *Arriagada et al.*, 2000] but no evidence of late Neogene rotations has been found [*Somoza et al.*, 1999; *Somoza and Tomlinson*, 2002]. In addition, although the tectonic uplift of the 3000–5000 m high ranges of the

[1]Departamento de Geología, IRD, Universidad de Chile, Santiago, Chile.
[2]UMR 6118 du CNRS, Géosciences-Rennes, Rennes, France.
[3]Servicio Nacional de Geología y Minería, Santiago, Chile.
[4]Now at SIPETROL, Santiago, Chile.
[5]Department of Geosciences, University of Arizona, Tucson, Arizona, USA.

0148-0227/03/2001JB001598$09.00

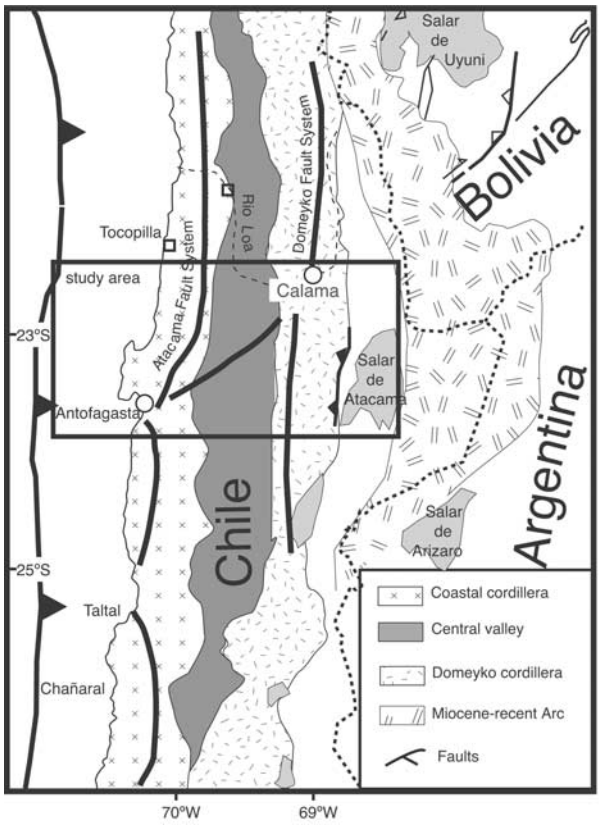

Figure 1. Simplified sketch of the Andes of northern Chile showing the principal morphologic units and main structural features. The large rectangle indicates the main study area further described in Figure 2. The small squares indicate the Tocopilla and Rio Loa sampling localities not shown in Figures 2, 4, and 5.

Domeyko Cordillera in northern Chile has been previously assumed to be mostly Miocene in age, fission track thermochronology [*Maksaev and Zentilli*, 1999] indicates that tectonic uplift and erosion were mainly active during the Eocene–early Oligocene, when at least 4–5 km of rocks were eroded during exhumation of tectonic blocks of the Domeyko Cordillera between ca. 45 and 30 Ma.

[5] In the Antofagasta region (Figure 1), most of the published paleomagnetic data have been obtained in upper Mesozoic rocks from the Coastal chain [*Turner et al.*, 1984; *Tanaka et al.*, 1988; *Forsythe and Chisholm*, 1994]. Here we report new paleomagnetic results based on extensive sampling in mostly volcanic rocks with occasional sedimentary, intrusive rocks, and semiconsolidated continental sediments across the forearc of the Antofagasta region (22°–24°S, Figures 1 and 2). The sampling includes Mesozoic rocks from the coastal chain, Cretaceous rocks from the Central Valley and Tertiary rocks from the western edge of the Domeyko Cordillera. Our study supplements results obtained by *Arriagada et al.* [2000] along the eastern border of the Cordillera de Domeyko.

2. Geology and Tectonics of the Forearc of Northern Chile

[6] In the forearc of northern Chile, subduction-induced magmatism has been active at least since 180 Ma [*Coira et al.*, 1982]. It is possible to distinguish four magmatic stages (Figures 2 and 3): a Jurassic–Early Cretaceous arc (180–120 Ma) in the Coastal Cordillera, a mid-Cretaceous arc (110–85 Ma) in the Central Valley, a latest Cretaceous (ca. 85–65 Ma) episode of volcanism in the central depression and an essentially Paleocene arc (65–55 Ma) along the western slope of the Cordillera de Domeyko [*Marinovic and García*, 1999; *Scheuber and González*, 1999; *Cortés*, 2000]. Magmatism in the forearc essentially ended during the Eocene to early Oligocene with emplacement of a suite of shallow stocks along the axis of the Domeyko Cordillera including some of the giant porphyry coppers of northern Chile [*Cornejo et al.*, 1997].

2.1. Geology of the Coastal Cordillera of the Antofagasta Region

2.1.1. Stratigraphy

[7] In the coastal Cordillera (Figures 2 and 3), a 3000–10,000 m thick volcanic sequence (La Negra Formation), composed mainly of subaerial lava and breccias of basaltic–andesitic composition, accumulated during Early to Middle Jurassic times. Associated intrusive bodies are of gabbroic to granodioritic composition. Subduction related plutonism started around 180 Ma and reached a maximum in Middle Jurassic to Early Cretaceous times (160–120 Ma) [*Boric et al.*, 1990].

2.1.2. Regional Structure

[8] The coastal magmatic arc is longitudinally cut by the Atacama Fault System (AFS, Figure 2). The AFS is a complex association of NS trending mylonitic and cataclastic zones and brittle faults exposed along the Coast Range of northern Chile, between 22°S and 29°S [*Hervé*, 1987; *Scheuber and Adriessen*, 1990; *Grocott et al.*, 1994; *Scheuber and González*, 1999]. The AFS has a long history of deformation spanning the Early Jurassic to Cenozoic.

[9] *Sheuber and González* [1999] suggested that structures of the Jurassic to Early Cretaceous magmatic arc formed in four stages. In Stage 1 (ca. 195–155 Ma), motion was left lateral and arc parallel. In Stage 2 (160–150 Ma), there was strong arc-normal extension. For Stage 3 (155–147 Ma), a reversal in the stress regime is indicated by two generations of dikes, an older one trending NE-SW and a younger one trending NW-SE. During Stage 4 (until ~125 Ma), left-lateral motions prevailed, the AFS originating as a left-lateral trench-linked fault. Brittle strike-slip and dip-slip movements continued intermittently along the AFS until the late Miocene [*Hervé*, 1987].

2.2. Geology of the Central Valley of the Antofagasta Region

2.2.1. Stratigraphy

[10] On the western side of the Central Valley (Figures 2, 3, and 4), scarce outcrops of upper Paleozoic sedimentary rocks are unconformably overlain by a marine sequence of Late Triassic to Early Jurassic age (Rencoret Formation) [*Cortés*, 2000] containing Hettangian–Sinemurian fossils. These sedimentary sequences are covered by andesitic rocks of the La Negra Formation. To the east, these andesitic rocks are not present but a mid-Cretaceous continental volcanic sequence (Paradero del Desierto Formation) [*Cortés*, 2000] is covered by the Late Cretaceous Quebrada Mala Formation (see below). Further east, along the western

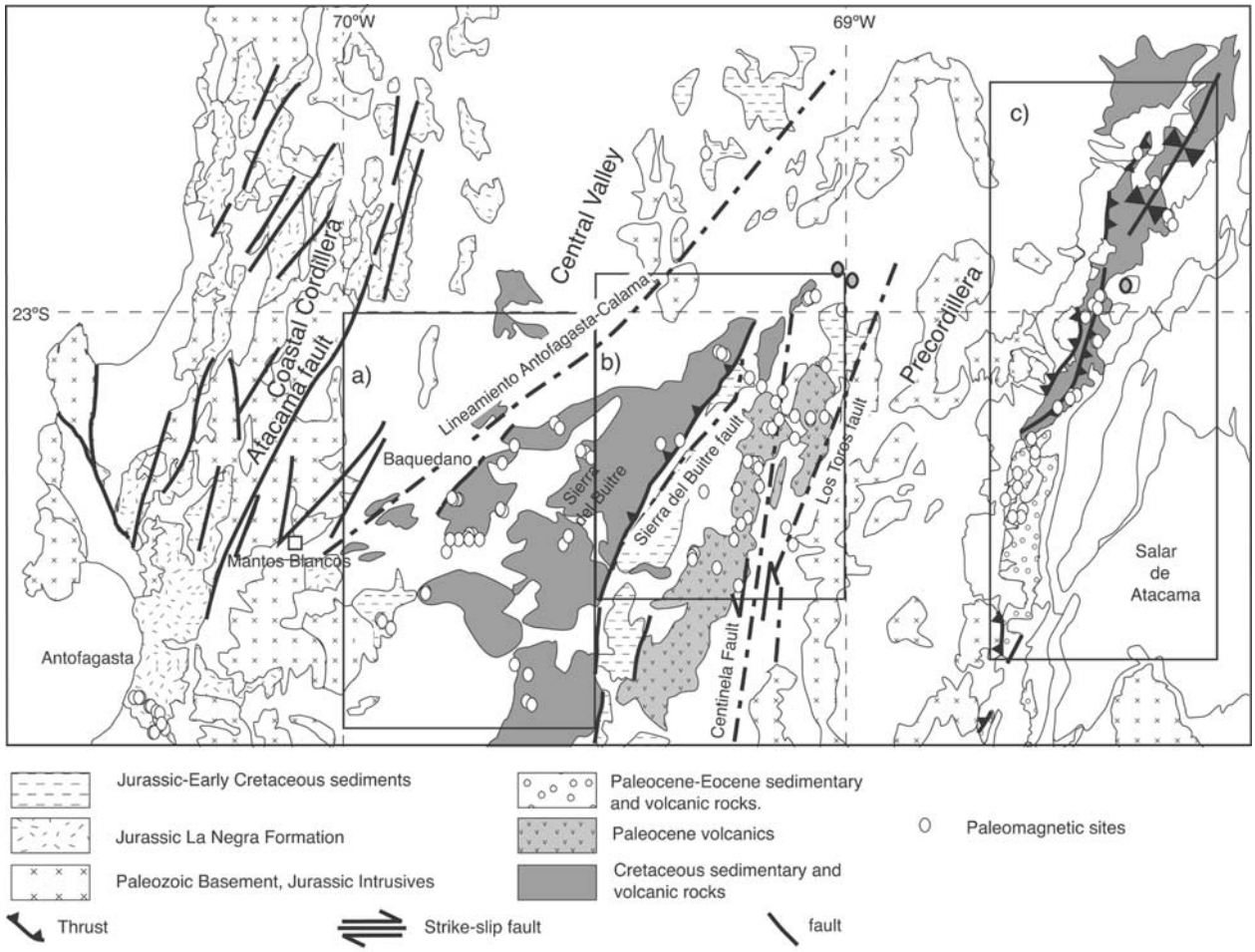

Figure 2. Geological map of the Antofagasta region showing paleomagnetic sites (modified after Mapa Geologico (1:1000.000), SERNAGEOMIN Chile) [*Marinovic and García*, 1999; *Arriagada et al.*, 2000; *Cortés*, 2000]. Rectangles a and b indicate the locations of the maps shown in Figures 4 and 5. Box c indicates the location of the paleomagnetic study previously published by *Arriagada et al.* [2000]. Circles indicate the location of the paleomagnetic sites (filled circles indicate the three sites in the Sifón Ignimbrite).

edge of the present-day Cordillera de Domeyko (Figures 2, 3, and 4), a thick sequence of Jurassic marine sediments (Caracoles Group) [*Marinovic and García*, 1999] accumulated in a long-lived back arc basin (Tarapaca basin) [*Mpodozis and Ramos*, 1990]. The upper part of the sequence consists of Upper Jurassic to Lower Cretaceous continental red beds. The Caracoles Group is overlain unconformably by continental sediments with interbedded volcanic sequences up to 3 km thick of the Quebrada Mala Formation, deposited between 85 and 65 Ma [*Marinovic and García*, 1999].

[11] In the Sierra del Buitre, the Mesozoic sequences are intruded by monzodiorites and granodiorites of the Sierra del Buitre Batholith (Figures 4 and 5). K-Ar and $^{39}Ar/^{40}Ar$ ages range at 74–66 Ma [*Cortés*, 2000]. To the east of the Sierra del Buitre (Figures 3, 4, and 5), the Mesozoic units are overlain by about 500 m of conglomerates, ignimbrites and andesitic lava flows of the Paleocene Cinchado Formation (63–55 Ma) [*Marinovic and García*, 1999]. Locally, the Cinchado Formation is covered by scarce andesitic lava flows and ignimbrites of the Cerro Casado Formation (48–45 Ma). Both units are separated by a smooth angular unconformity.

2.2.2. Regional Structure

[12] The Central Valley is traversed by several NE-NNE striking faults and lineaments (Figures 2, 4, and 5). The most important structural feature is a major lineament parallel to the Antofagasta–Calama road and here termed the Lineamiento Antofagasta–Calama (Figures 2, 4, and 5). To the SE of the Lineamiento Antofagasta–Calama, the Sierra del Buitre is a structurally uplifted block consisting mainly of Mesozoic rocks. The Sierra del Buitre fault (Figure 5), a SE verging imbricate reverse fault lying immediately east of the Sierra del Buitre, places the Quebrada Mala Formation over the Caracoles Group. It probably originated as a normal fault and was later reactivated as an inverse fault during inversion of the Quebrada Mala basin in the latest Cretaceous–early Paleocene [*Marinovic and García*, 1999].

[13] The Mesozoic rocks were deformed in several stages of Cretaceous compression. Deformation in the Caracoles Group is marked by open plunging folds and is especially

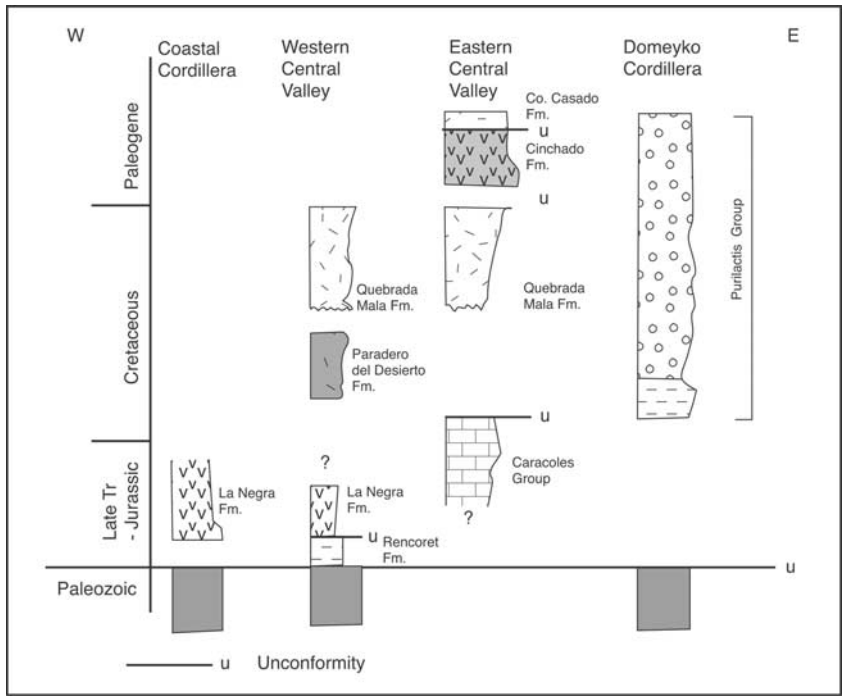

Figure 3. Simplified stratigraphy between Coastal Cordillera and Domeyko Cordillera including the principal names of geological formations described in the text (modified *after* the studies of *Marinovic and García* [1999], *Arriagada et al.* [2000], and *Cortés* [2000].

significant within limestones and evaporites. At least part of the deformation of the Caracoles group predates the accumulation of the Quebrada Mala Formation which is in turn deformed by predominantly symmetrical folds, with subhorizontal axes trending N10°–N50°E. Finally, the Cinchado Formation is deformed only by open folds with amplitudes of several hundred meters. Deformation is not observed everywhere. For example, to the east of Sierra del Buitre (near site CG02), a horizontal volcanic flow of the Cinchado Formation overlies an eroded paleosurface carved in horizontal Jurassic limestones of the Caracoles Group.

2.3. Geology of the Cordillera de Domeyko in the Antofagasta Region

2.3.1. Stratigraphy

[14] The Domeyko range consists mainly of upper Paleozoic plutonic and volcanic rocks, which are devoid of any Mesozoic cover [*Coira et al.*, 1982; *Reutter and Scheuber*, 1988; *Mpodozis et al.*, 1993]. At the eastern edge of the Domeyko range, the Paleozoic basement overthrusts, or is overlain unconformably by, a sequence of red beds and interbedded volcanics, up to 5 km thick, deposited during the Early Cretaceous to Eocene (Figures 2 and 3). They have been described as the Purilactis Group [*Charrier and Reutter*, 1994; *Arriagada et al.*, 2000], and have been interpreted as the infill of a large basin. This basin formed under the modern Salar de Atacama, and was connected, to the east, with the Salta Group rift basins of northwestern Argentina [*Grier et al.*, 1991].

2.3.2. Regional Structure

[15] The Domeyko range is a narrow mountain range lying between the pre–Andean Depression and the Salar de Atacama basin, to the east, and the Central Depression (Central Valley, Figure 2), to the west. The major structural feature in the Domeyko range is the Domeyko Fault System (DFS). Transpressional and left-lateral displacements in the DFS have been documented in the late Eocene and possibly into the early Oligocene to the south of Calama, although offsets probably did not exceed ~2 km [*Mpodozis et al.*, 1993; *Tomlinson et al.*, 1994]. To the north of Calama, however, the Eocene (Incaic) deformation is represented by a set of west and east verging faults, which have uplifted basement blocks and show no significant component of strike-slip [*Tomlinson and Blanco*, 1997a]. By the end of the early Oligocene (after ~31 Ma), a period of left-lateral displacement has been well documented for the area north of Calama (Figure 1), resulting in a net offset of approximately 35 km in the Chuquicamata–El Abra area, ensued up to the middle Miocene (~17 Ma) [*Reutter et al.*, 1996; *Dilles et al.*, 1997; *Tomlinson and Blanco*, 1997b].

[16] In the region west of the Salar de Atacama (Figure 2), the Domeyko range is bounded to the west by the N-S trending Centinela Fault (Figure 5), which has been interpreted as a "master fault" of the DFS [*Mpodozis et al.*, 1993]. Left-lateral strike-slip movements can be inferred from a compressive duplex exposed along the northern part of this fault [*Marinovic and García*, 1999]. To the east of the Centinela Fault, the Cinchado Formation and Caracoles Group are separated from Paleozoic units by the N30°E trending Los Toros Fault. This fault has been interpreted as a secondary structure of the Centinela fault [*Marinovic and García*, 1999].

3. Paleomagnetic Method

3.1. Paleomagnetic Sampling

[17] Paleomagnetic sampling was done during several field trips and a total of 108 sites were sampled. For most sampling, we used a portable gasoline-powered drill with a

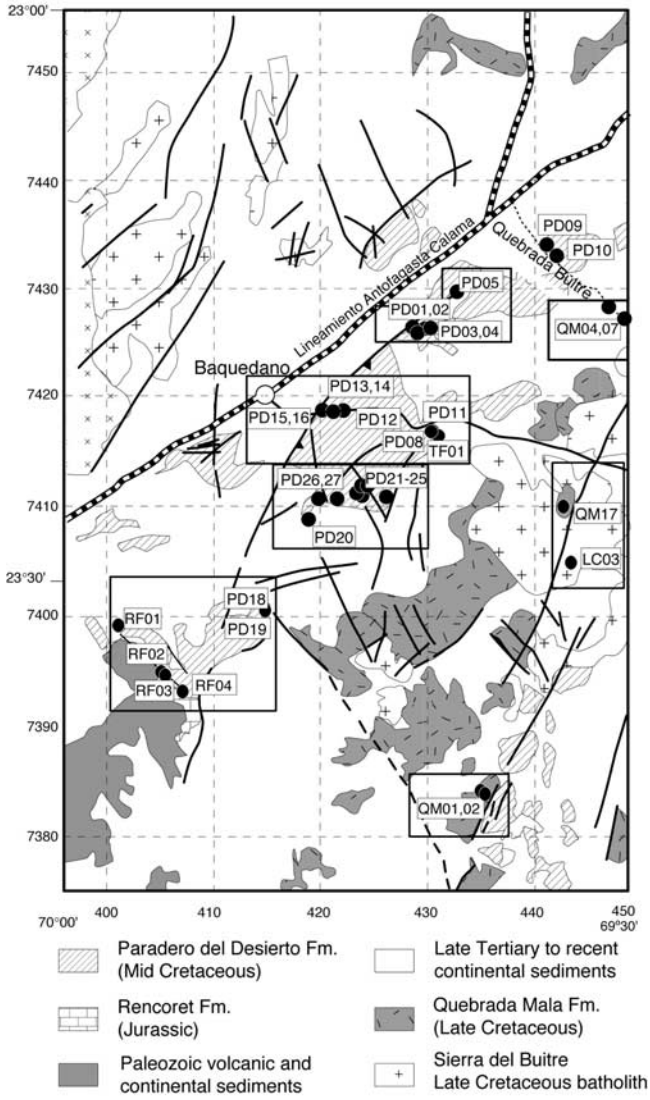

Figure 4. Geology of the Baquedano Area, western Central Valley, and paleomagnetic sites (modified after the studies of *Marinovic and García* [1999] and *Cortés* [2000]).

water-cooling system. For weakly lithified layers, we used an air-cooled system. Samples were oriented using magnetic and solar compasses. The locations of paleomagnetic sites are given in Table 1 and shown in Figures 2, 4, and 5. We sampled the Jurassic La Negra Formation near coastal localities: Tocopilla (13 sites) and Antofagasta (17 sites). Near Antofagasta, the thickness of the sampled section is larger than 3000 m. The sampling is not in a continuous section near Tocopilla.

[18] Within the Central Valley and the Domeyko range most samples are from Cretaceous and Paleocene–Eocene volcanics, whereas a few are from Jurassic marine sediments, Mesozoic sandstones, and Upper Cretaceous to Eocene intrusives. To get an upper constraint on the age of rotations in the forearc, 2 sites in semiconsolidated Oligocene–Miocene continental sediments, and 3 sites in a Miocene ignimbritic flow (Sifón Ignimbrite) were also sampled (Figures 1, 2, and 5).

[19] Sites in volcanic rocks include samples from a single flow, dyke, sill or ignimbrite. Secular variation was thus not averaged at these single-bed sites. In contrast, in sedimentary rocks, sampling included different beds across several meters of stratigraphic section. In such few sites the site-mean paleomagnetic direction should average the secular variation and provide a good estimate of tectonic rotations. Where sediments were not interbedded with volcanics, bedding corrections for volcanic rocks were estimated from general flow attitudes. A few sites were drilled in intrusive rocks. Except at one site (LC02), bedding of the surrounding rocks is almost flat.

3.2. Paleomagnetic Techniques

[20] Samples were analyzed in paleomagnetic laboratories at the University of Chile and the University of Rennes. Remanent magnetization was measured with either a spinner magnetometer (Molspin or AGICO JR5A) or a cryogenic magnetometer (CEA-LETI). Magnetic susceptibility was measured with a Bartington susceptibility meter. To better constrain the magnetic mineralogy, we studied the acquisition of isothermal remanent magnetization (IRM) and the variation of susceptibility during heating (K-T) on characteristic samples. IRM was given with a pulse electromagnet and K-T experiments were done with the AGICO KLY3-CS3 instrument.

[21] For most samples, one specimen was subjected to stepwise thermal demagnetization (10–15 steps) in an

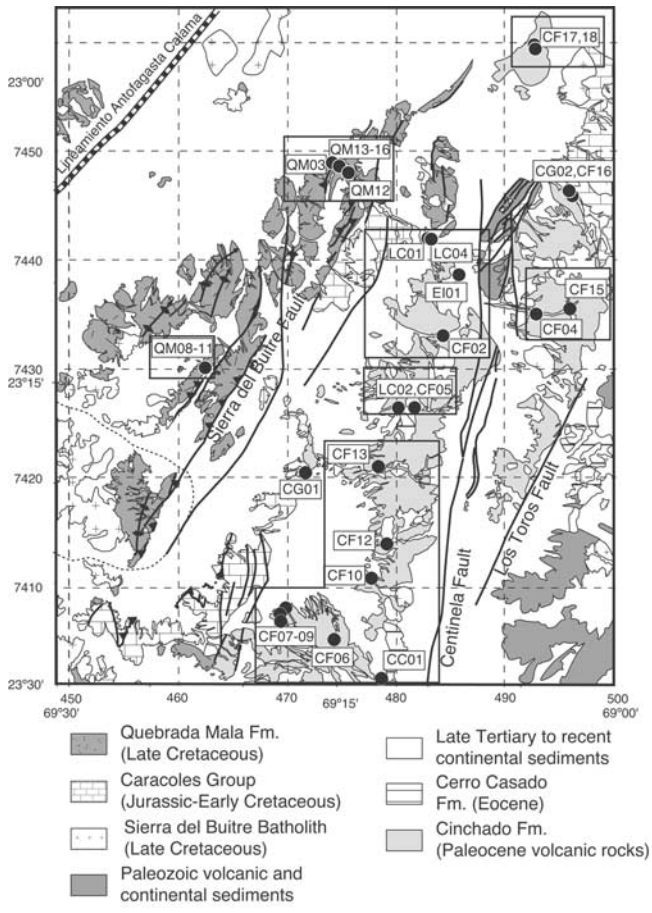

Figure 5. Geology of the Sierra del Buitre Area, eastern Central Valley, and paleomagnetic sites (modified after modified after the study of *Marinovic and García* [1999]).

Table 1. Location of the Paleomagnetic Sampling and Magnetic Properties

Site	Lithology	Latitude (°S)	Longitude (°W)	NRM (A/m)	K (SI)	Strike/Dip
		La Negra Formation (Jurassic) Tocopilla				
LN01	Lava flow	22°11.6	70°13.33	0.42	0.045	0/30
LN02	Lava flow	22°11.52	70°13.48	0.19	0.057	0/30
LN03	Lava flow	22°11.53	70°13.42	0.29	0.052	0/30
LN04	Lava flow	22°9.07	70°13.32	0.47	0.052	0/30
LN05	Lava flow	22°17.52	70°14.45	0.21	0.036	0/30
LN06	Breccia/ oxidized	22°17.52	70°14.50	0.1	0.0013	0/30
LN07	Lava flow	22°17.50	70°14.50	0.25	0.063	0/30
LN08	Lava flow	22°17.50	70°14.50	0.48	0.054	0/30
LN09	Lava flow	22°22.22	70°15.00	0.36	0.069	0/30
LN10	Lava flow	22°22.15	70°14.70	0.39	0.071	0/30
LN11	Lava flow	22°22.1	70°14.57	0.39	0.065	0/30
LN12	Lava flow	22°22.1	70°14.57	0.48	0.069	0/30
LN13	Diorite	22°05.95	70°7.18	0.078	0.022	
		La Negra Formation (Jurassic) Antofagasta				
LN14	Lava flow	23°45.42	70°20.95	0.11	0.022	205/35
LN15	Lava flow	23°45.1	70°21.57	0.17	0.031	160/30
LN16	Lava flow	23°44.83	70°21.39	0.035	0.011	180/30
LN17	Lava flow	23°44.40	70°21.68	0.095	0.023	160/30
LN18	Lava flow	23°43.53	70°21.97	0.15	0.029	180/40
LN19	Sill	23°42.86	70°22.76	0.086	0.015	170/40
LN20	Lava flow	23°41.98	70°23.85	0.061	0.011	170/40
LN21	Ryolite	23°41.97	70°24.63	0.033	0.00023	170/40
LN22	Ryolite	23°41.97	70°24.63	0.011	0.00004	170/40
LN23	Lava flow	23°41.95	70°23.88	0.042	0.0063	170/40
LN24	Lava flow	23°45.75	70°22.3	0.21	0.024	170/40
LN25	Lava flow	23°45.76	70°22.23	0.059	0.0094	170/45
LN26	Lava flow	23°42.94	70°22.58	0.16	0.028	190/45
LN27	Lava flow	23°43.53	70°21.97	0.14	0.035	180/40
LN28	Lava flow	23°43.74	70°21.5	0.36	0.060	190/45
LN29	Lava flow	23°44.83	70°21.39	0.47	0.039	190/45
LN30	Lava flow	23°44.83	70°21.39	0.17	0.016	180/30
		Rencoret Formation (Early Jurassic)				
RF01	Limestone/oxidized	23°31.10	69°57.85	0.00671	0.000115	259.3/24.9
RF02	Limestone/oxidized	23°33.47	69°55.45	0.00387	6.17e−05	292.4/25.2
RF03	Limestone/oxidized	23°33.62	69°55.31	0.00591	0.000108	273.5/11.3
RF04	Limestone/oxidized	23°34.30	69°54.23	0.0178	0.000193	331.1/24
		Caracoles Group (Jurassic)				
CG01	Siltstone/oxidized	23°19.60	69°16.70	0.0366	0.000167	246.4/34.3
CG02	Limestone	23°5.51	69°2.47	0.000889	8.98e−05	243/4
		Paradero del Desierto Formation (mid-Cretaceous)				
PD01	Lava flow	23°16.48	69°41.54	0.136	0.00299	100/30
PD02	Lava flow	23°16.29	69°41.75	0.561	0.00127	100/30
PD03	Lava flow	23°16.34	69°41.10	0.569	0.0329	100/30
PD04	Ignimbritic flow	23°16.24	69°40.74	0.121	0.00111	100/30
PD05	Dyke	23°14.38	69°39.36	0.472	0.00463	Subvert.
PD06	Lava flow	23°42.45	69°38.13	0.133	0.01	250/40
PD07	Lava flow	23°42.84	69°37.49	0.154	0.00171	259.6/36.8
PD08	Lava flow	23°21.62	69°40.51	0.0952	0.000407	Subhoriz.
PD09	Lava flow	23°11.95	69°34.58	0.924	0.0127	Subhoriz.
PD10	Lava flow	23°12.44	69°33.91	0.175	0.0285	Subhoriz.
PD11	Ignimbritic flow	23°21.41	69°40.96	0.379	0.000944	Subhoriz.
PD12	Dyke	23°20.28	69°45.95	0.184	0.0278	145/16
PD13	Lava flow/oxidized	23°20.52	69°46.22	0.0446	0.000329	145/16
PD14	Limestone/oxidized	23°20.23	69°46.57	0.00795	0.000109	138/17
PD15	Lava flow/oxidized	23°20.20	69°46.57	0.0705	0.000595	155/32
PD16	Lava flow/oxidized	23°20.20	69°46.57	0.0546	0.000853	155/32
PD18	Sandstone/breccias	23°30.41	69°49.99	0.0175	0.0004	40/30
PD19	Lava flow	23°30.52	69°49.98	0.033	0.000405	40/30
PD20	Lava flow	23°26.01	69°47.60	0.38	0.00803	327/17
PD21	Lava flow	23°24.05	69°44.48	0.754	0.0256	Subhoriz.
PD22	Lava flow	23°24.06	69°44.78	0.0211	6.39e−05	Subhoriz.
PD23	Lava flow	23°24.45	69°45.05	1.11	0.0251	Subhoriz.
PD24	Lava flow	23°24.67	69°43.45	0.275	0.00132	180/10
PD25	Lava flow	23°24.59	69°44.73	0.54	0.0186	Subhoriz.
PD26	Lava flow	23°24.79	69°46.15	1.77	0.0204	45/5
PD27	Lava flow	23°24.74	69°47.14	0.27	0.0295	45/5

Table 1. (continued)

Site	Lithology	Latitude (°S)	Longitude (°W)	NRM (A/m)	K (SI)	Strike/Dip
			Quebrada Mala Formation (Late Cretaceous)			
QM01	Ignimbritic flow	23°39.57	69°37.87	0.0229	0.000138	76.7/43.1
QM02	Ignimbritic flow	23°39.49	69°38.15	0.631	0.000295	27.2/32.8
QM03	Lava flow	23°4.093	69°15.17	1.45	0.0162	204/63.8
QM04	Lava flow	23°15.25	69°30.89	0.175	0.00136	Subhoriz.
QM05	Lava flow	23°15.02	69°31.43	0.0424	0.00051	222/12
QM06	Ignimbritic flow	23°15.02	69°31.43	0.0318	1.36e−05	222/12
QM07	Lava flow	23°15.69	69°30.33	0.507	0.0127	Subhoriz.
QM08	Ignimbritic flow	23°14.26	69°22.06	0.112	0.00548	216.6/82.6
QM09	Ignimbritic flow	23°14.26	69°22.06	0.256	0.000425	216.6/82.6
QM10	Ignimbritic flow	23°14.26	69°22.06	0.0947	0.0193	216.6/82.6
QM11	Ignimbritic flow	23°14.25	69°22.07	0.343	0.0187	216.6/82.6
QM12	Ignimbritic flow	23°4.57	69°14.28	0.134	0.000304	184.4/87
QM13	Ignimbritic flow	23°4.26	69°14.80	0.265	0.000939	211/74
QM14	Ignimbritic flow	23°4.26	69°14.80	0.0862	0.00047	211/74
QM15	Ignimbritic flow	23°4.26	69°14.80	0.322	0.00129	211/74
QM16	Ignimbritic flow	23°4.26	69°14.80	0.0347	0.000315	211/74
QM17	Tuffaceous sediments	23°25.26	69°33.69	0.455	0.000906	210.8/10
			Late Cretaceous intrusives			
LC01	Diorite	23°7.915	69°9.984	0.0295	0.00506	
LC02	Diorite	23°16.32	69°10.77	0.63	0.00607	
LC03	Diorite	23°28.17	69°33.32	1.17	0.0179	
LC04	Diorite	23°7.983	69°9.865	0.488	0.0166	
			Cinchado Formation (Paleocene)			
CF01	Lava flow	23°7.915	69°9.984	0.275	0.0431	Subhoriz.
CF02	Lava flow	23°12.68	69°9.256	0.137	0.00862	205.7/25.3
CF03	Lava flow	23°13.64	69°6.112	1.24	0.00287	Subhoriz.
CF04	Lava flow/oxidized	23°11.61	69°4.252	1.2	0.0074	156/25
CF05	Ignimbritic flow	23°16.23	69°11.59	0.21	0.00163	240.6/60
CF06	Ignimbritic flow	23°27.96	69°15.15	0.134	0.00186	150.2/41.5
CF07	Ignimbritic flow	23°26.37	69°17.78	0.194	0.00265	148.8/14.6
CF08	Tuffaceous sediments	23°26.67	69°18.10	0.0614	8.57e−05	80/20
CF09	Ignimbritic flow	23°27.04	69°18.06	0.0068	6.13e−05	20/15
CF10	Lava flow	23°24.89	69°13.12	4.72	0.00693	110.4/27.4
CF11	Ignimbritic flow	23°22.43	69°11.46	0.259	0.0129	160/70
CF12	Lava flow	23°23.17	69°12.30	1.23	0.00116	110/15
CF13	Ignimbritic flow	23°19.28	69°12.75	0.621	0.00137	129.3/24.2
CF14	Tuffaceous sediments	23°19.02	69°10.09	1.49	0.000306	145/40
CF15	Lava flow	23°11.37	69°2.352	0.132	0.0224	180/20
CF16	Lava flow	23°5.66	69°2.40	2.0	0.0297	Subhoriz.
CF17	Lava flow	22°58.46	69°4.614	1.34	0.000157	165/15
CF18	Lava flow	22°58.24	69°4.274	0.0779	0.00117	150/30
			Eocene intrusive			
EI01	Diorite	23°9.646	69°8.385	0.519	0.0278	
			Cerro Casado Formation (Eocene)			
CC01	Ignimbritic flow	23°29.95	69°12.52	2.64	0.0108	Subhoriz.
			Tambores Formation or Atacama gravels (Miocene)			
TF01	Sandstone	23°21.41	69°40.91	0.0744	0.00302	Subhoriz.
			El Loa Formation (Oligocene–Miocene)			
LF01	Siltstones	21°37.59	69°32.57	0.0337	0.00198	Subhoriz.
			Sifon ignimbrite (Miocene)			
SI01	Ignimbritic flow	22°56.89	68°26.66	0.193	0.00772	Subhoriz.
SI02	Ignimbritic flow	22°53.45	69°1.111	0.313	0.00115	Subhoriz.
SI03	Ignimbritic flow	22°56.44	68°58.34	0.0493	0.00266	Subhoriz.

Sites coordinates, NRM: Geometric mean intensity of remanent magnetization. K: Geometric mean susceptibility. Strike and dip: Bedding attitude parameters.

ASC Scientific furnace where the residual field was less than 10 nT. Magnetic susceptibility was measured after each thermal demagnetization step, in order to check magnetic mineralogical changes upon heating. To better investigate the origin of the remanent magnetization, stepwise alternating field (AF) demagnetization using the Molspin AF instrument was also performed on some samples. AF demagnetization was preferred to thermal, only where there was evidence of remagnetization by lightning. Magnetization directions were determined with ''least squares lines and planes'' programs according to *Kirschvink* [1980]. Evidence for secondary overprint due to lightning was found at a few sites in volcanic rocks. Statistics combining directions and planes [*McFadden and*

McElhinny, 1988] were used to determine the mean characteristic directions for such sites.

3.3. Reference Poles

[22] The motion of South America since the early Mesozoic has been mostly an E-W displacement with successive small clockwise or counterclockwise rotations. This behavior leads to an APWP positioned close to the present-day geographic axis. Except for the Early Cretaceous (Paraná Volcanics) [*Ernesto et al.*, 1990; *Raposo and Ernesto*, 1995] very precise paleomagnetic reference poles are lacking for the South American plate.

[23] *Roperch and Carlier* [1992] suggested that the best approach for a South American reference curve was to transfer the master curve defined by *Besse and Courtillot* [1991] to the South American plate. *Beck* [1999] criticized this approach and suggested that the APWP variations are small enough for a single pole to be calculated for the whole Mesozoic. *Lamb and Randall* [2001] developed a technique allowing paleomagnetic poles to be calculated from a mixture of declination and inclination data drawn from localities in stable South America and in the Andes. *Lamb and Randall* [2001] also attempted to correct for compaction in sedimentary rocks. The APWP obtained following this interesting approach is not significantly different from the one given by *Roperch and Carlier* [1992] and this demonstrates that an APWP for South America can be determined. *Besse and Courtillot* [2002] have updated several APWPs for most continents. We believe that their new SA APWP (hereafter labeled BC01) is the most reliable APWP and that it should henceforth be used to calculate tectonic rotations. Because of the age uncertainties of the rock formation, we will use the BC01 APWP calculated through a 20 Ma running window.

[24] The lack of geological evidence for large latitudinal displacements in the Andes suggests that our study area has been more or less (within 1°) stable in latitude relative to South America. Comparison of the observed inclinations, in volcanic rocks and remagnetized units (see below), with the expected inclination calculated from the BC01 APWP confirms that no significant latitudinal displacements can be demonstrated.

4. Magnetic Properties and Characteristic Directions

[25] For most samples, except from Jurassic rocks, interpretation of demagnetization data was straightforward and the primary or secondary origin of the characteristic remanent magnetization (ChRM) was well defined for each site. Mostly, the Fisher concentration parameter is higher than 100 and the 95% confidence angle is lower than 5°. The magnetic properties are mainly deduced from progressive thermal or alternating field demagnetizations and measurements of magnetic susceptibility after each step of thermal treatment.

[26] As shown in Table 1, there is a large dispersion in the site-mean values of magnetic susceptibility and intensity of natural remanent magnetization (NRM). NRM intensities are between 0.0008 and 6 A/m while volume magnetic susceptibility varies between 0.00001 and 0.1 SI. These large variations are correlated to changes in lithology. Magnetite and maghemite are the main magnetic carriers of the NRM for sites where magnetic susceptibility is higher than 0.005 SI. Usually, hematite is the main magnetic carrier of the NRM for the highly oxidized rocks. This is especially so for some ignimbrites where oxidation probably occurred during emplacement. At a few localities, field evidence for a late phase of oxidation corroborates paleomagnetic evidence for remagnetization.

4.1. La Negra Formation: Coastal Area

[27] Magnetic susceptibility is mostly high to very high (up to 0.1 SI, Table 1), especially in the Tocopilla area where the Jurassic volcanics are characteristically rich in magnetite. Multidomain magnetite and maghemite are often the main magnetic carriers and secondary magnetizations are widespread. 108 samples were subjected to low temperature demagnetization by cooling in zero field down to liquid nitrogen temperature. This process was efficient in removing part of the secondary overprint associated with multidomain magnetite.

[28] In the Antofagasta area, where low-grade metamorphism is important, normal and reverse polarity magnetizations are often found within the same flow. However, at some sites, samples from the interior part of the lava record a well-defined magnetization, unblocking temperatures being higher than 500°C. In contrast, the brecciated and vesicular part of the lava yield a more complex record of remanent magnetization (Figures 6a and 6b, site LN18).

[29] At some sites, apparent antiparallel magnetizations are observed without clear evidence of significant differences in secondary mineral assemblages (Figures 6c–6e, site LN25). As the volcanics near Antofagasta have the same bedding attitude toward the west, it is not possible to perform a true fold test. The fact that the in situ ChRM directions carried by samples showing low temperature alteration is closer to the tilt-corrected directions of the unaltered samples is an indication that low temperature metamorphism in these rocks is probably later than tilting. Dikes intruding Upper Jurassic plutons in the same area are vertical. This indicates that the plutons, which are younger than La Negra volcanics, are not tilted and could have remagnetized the volcanics after the deformation. Because it is uncertain whether or not a tilt correction should be applied to the secondary magnetization, we will not consider these magnetizations as valid for tectonic purposes.

[30] Two sites were drilled in the upper level of the volcanic pile, one in a red rhyolite overlain by a welded ignimbrite (sites LN21 and LN22, Table 1). In contrast to the magnetic behavior of most of the andesitic lavas of the La Negra Formation, these rocks are highly oxidized and the ChRM is carried by hematite. However, the two successive units show opposite polarities, indicating that oxidation is of primary origin.

[31] The between-site dispersion is high, suggesting high secular variation of the Earth's magnetic field during the Jurassic (Figure 6f). Dispersion decreases slightly upon tilt correction. The mean direction (Table 2) is similar to the expected direction calculated with the 180 Ma pole of the BC01 APWP.

4.2. Rencoret Formation: Central Valley

[32] Samples from oxidized Lower Jurassic limestones (Rencoret locality (RF01-04)) from the Central Valley of the

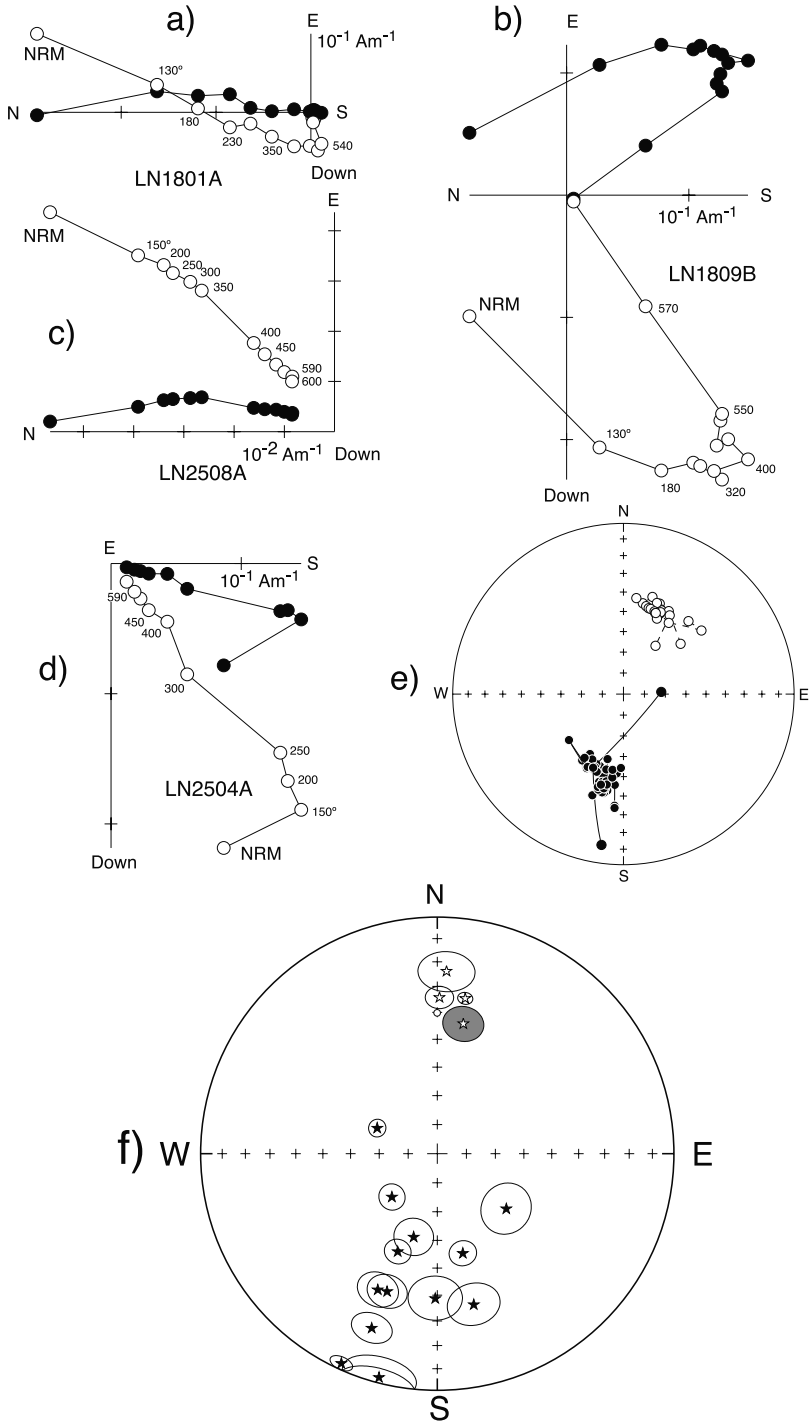

Figure 6. Orthogonal projections (in situ) of thermal demagnetization diagrams for samples in volcanic rocks of La Negra Formation. The reverse component of magnetization with high unblocking temperature observed in sample LN1809B cannot be isolated in the more intensely altered sample LN1801A from the same flow LN18. Both normal (c) and reverse (d) magnetizations are found within the same flow (LN25). (e) In equal-area projection of the demagnetization data for all samples of this site, we can observe antipodal magnetizations. Solid (open) circles correspond to projection into the horizontal (vertical) plane. (f) Equal-area projection of site-mean characteristic directions in tilt corrected coordinates from La Negra Formation (Table 2). The stars with the 95% error angle of confidence indicate the expected direction calculated from the BC01 APWP.

Table 2. Paleomagnetic Results

Site	N/n	In situ Dec	In situ Inc	α95	k	Tilt corrected Dec	Tilt corrected Inc	Locality
Jurassic: La Negra Formation								
Tocopilla								
LN01	14/14	19.6	−29.2	4.3	88	0.8	−34.3	15
LN02	10/11	216.3	23.7	6.3	62	200.0	38.0	15
LN03	7/7	206.5	51.1	4.5	193	165.6	54.2	15
LN05	8/9	195.4	71.1	8.7	41	128.6	59.4	15
LN06	11/11	203.1	−9.1	3.0	239	204.6	2.9	15
LN07	6/9	194.0	−4.7	9.4	63	194.6	2.6	15
LN08	7/10	202.6	32.7	8.4	59	180.8	38.7	15
LN12	9/9	229.1	43.2	6.6	75	195.8	60.0	15
Antofagasta								
LN18	8/12	149.1	48.6	4.4	174	202.0	53.2	16
LN19	9/11	144.1	23.0	8.1	46	166.4	34.7	16
LN21	9/9	341.7	−34.4	2.3	496	10.2	−33.7	16
LN22	6/6	179.3	33.2	6	719	200.6	22.3	16
LN23	5/7	343.7	−25.3	8.2	100	2.9	−23.8	16
LN26	13/13	131.9	53.8	4.5	95	226.3	68.4	16
LN27	10/10	169.2	41.2	6.5	64	203.6	37.3	16
LN28[a]	11/11	89.7	66.7	3.0	252	293.1	67.5	16
mean	15/16	3.9	−36.4	15.3	7			
mean	15/16			**12.0**	**11**	**9.1**	**−39.2**	
Early Jurassic: Rencoret Formation								
RF01	10/10	24.8	−47.8	2.4	405	54.2	−64.2	1
RF02	8/8	33.3	−44.8	3.4	273	44.4	−69.1	1
RF03	10/10	31.3	−50.1	5.3	85			
				10.1	24	19	−58.4	1
RF04	12/16	32.9	−40.6	1.7	646	15.1	−60.1	1
mean		**30.7**	**−45.9**	**5.6**	**270**			
				11.2	68	31.3	−63.9	
Mid-Cretaceous: Paradero del Desierto Formation								
PD18	9/12	53.0	−47.6	7.5	48	20.1	−45.6	1
PD19	7/7	57.4	−42.9	5.7	114	27.8	−44.4	1
PD20	9/9	64.0	−36.7	2.0	702	66.4	−53.5	2
PD21	9/10	47.4	−45.1	5.9	76	47.4	−45.1	2
PD22	10/10	25.9	−21.7	4.3	128	25.9	−21.7	2
PD23	10/10	40.6	−51.5	2.1	536	40.6	−51.5	2
PD24	11/11	23.5	−49.2	3.6	166	32.9	−44.5	2
PD25	13/13	39.9	−50.8	5.4	59	39.9	−50.8	2
PD26	9/9	65.4	−46.8	4.3	146	60.2	−48.4	2
PD27	7/7	59.0	−33.6	8.0	57	55.7	−34.7	2
PD08	6/7	34.4	−38.8	3.5	363	34.4	−38.8	3
PD11	9/9	54.2	−48.0	2.1	588	54.2	−48.0	3
PD12	8/8	41.3	−49.9	2.8	431	44.3	−34.7	3
PD13	10/10	37.4	−61.0	2.3	452	42.9	−45.9	3
PD14	4/5	54.9	−57.8	5.9	330	52.9	−40.6	3
PD15	15/19	53.2	−61.8	1.8	465	58.5	−30.3	3
PD16	13/13	45.5	−68.3	2.2	371	56.0	−37.3	3
PD01	8/8	68.9	−76.7	2.1	699	28.5	−51.6	4
PD02	9/9	60.6	−76.9	1.5	1127	26.0	−50.5	4
PD03	9/10	47.8	−62.9	2.9	313	30.2	−36.2	4
PD04	8/9	88.2	−75.9	3.7	226	34.3	−54.6	4
PD05	8/8	50.7	−56.5	3.6	238	50.7	−56.5	4
mean	22/22	48.4	−53.5	6.4	25			
				5.0	**40**	**42.2**	**−44.6**	
Late Cretaceous: Quebrada Mala Formation and related intrusives								
QM01	6/7	47.3	−55.8	11.6	34	19.1	−24.7	5
QM02	9/12	51.3	−41.9	5.9	78	18.3	−46.7	5
QM17	6/6	3.0	−55.8	5.6	144	17.8	−59.3	6
LC03	7/7	28.2	−54.5	5.1	161	28.2	−54.5	6
QM04	9/12	223.9	50.1	5.8	80	223.9	50.1	7
QM05	7/10	182	11.4	4.4	219	184.5	18.7	7
QM06	9/9	181.0	18.4	9.9	28	184.7	25.7	7
QM07	11/12	13.9	−45.4	3.1	233	13.9	−45.4	7
QM08	5/5	326.4	−2.1	6.1	156	22.7	−69.6	8
QM09	9/9	349.3	16.4	4.1	160	6.9	−41.5	8
QM10	5/5	334.1	21.6	5.4	202	349.0	−50.4	8
QM11	6/8	330.5	24.5	4.0	356	342.0	−50.5	8
QM03	5/5	307.5	−21.0	5.8	172	4.6	−76.1	9
QM12	8/8	338.1	−17.3	3.1	329	22.2	−26.0	9
QM13	9/9	337.2	−19.9	2.7	372	43.7	−55.4	9
QM14	6/6	306.5	−18.2	3.7	325	58.9	−84.2	9
QM15	8/8	314.8	−21.7	3.4	273	58.5	−75.7	9
QM16	8/8	333.1	−3.8	4.2	173	13.9	−56.4	9
mean	18/18	350.1	−26.6	16.5	5			
				9.5	**14**	**15.6**	**−51.9**	
Paleocene: Cinchado Formation and related intrusives								
CF04	4/4	216.9	66.2	4.1	501	230.2	42.8	10
CF15	6/7	208.2	49.1	2.8	987	223.2	36.8	10
CF02	5/5	194.8	38.5	12.0	175	215.6	38.4	11
LC01	8/9	207.6	51.2	10.1	34	207.6	51.2	11
LC04	8/10	29.3	−52.3	5.7	100	29.3	−52.3	11
EI01	6/8	200.2	37.7	11.1	40	200.2	37.7	11
CF06	9/9	14.8	−72.2	6.2	70	43.9	−34.6	12
CF07	5/5	45.5	−56.4	3.9	376	48.6	−42.0	12
CF08	7/9	35.0	−51.3	3.6	275	22.6	−35.8	12
CF09	5/7	36.8	−40.0	11.3	47	23.7	−43.1	12
CF10	6/7	229.7	62.7	5.3	173	216.2	37.4	12
CF12	10/10	230.0	74.6	2.8	308	215.0	60.8	12
CF13	6/8	217.4	55.7	4.4	230	217.6	31.5	12
CC01	5/5	24.8	−46.1	8.1	104	24.8	−46.1	12
CF05	6/11	0.7	25.5	11.1	37	1.9	−29.1	13
LC02	4/6	181.5	40.6	8.5	117	181.5	40.6	13
CF17	6/6	198.8	53.3	4.3	248	211.8	43.5	14
CF18	5/7	193.5	67.1	5.5	298	217.8	41.6	14
CF16	9/10	15.3	−51.0	7.1	64	15.3	−51.0	
mean	19/19	24.5	−51.3	9.4	14			
				5.4	**39**	**29.8**	**−42.7**	
Oligocene–Miocene Tambores Formation								
TF01	9	178.7	33.1	n.d	n.d	178.7	33.1	
Oligocene–Miocene El Loa Formation								
LF01	17/21	352.7	−25.5	5.9	37.8	352.7	−25.5	
Jurassic: Caracoles Group								
CG01	7/8	44.2	−24.2	7.0	80	62.5	−31.4	
CG02	9/13	10.2	−44.5	8.6	37	12.8	−47.6	
Sifon ignimbrite								
SI01	10/10	358.3	17.7	2.9	286	358.3	17.7	
SI02	7/11	6.8	35.8	6.3	106	6.8	35.8	
SI03	9/12	3.8	35.6	16.2	13	3.8	35.6	

N/n: Number of samples used in the calculation of the mean direction/number of demagnetized samples. Dec, Inc: Mean declination and inclination in situ and after tilt correction. α95: Semiangle of 95% of confidence. k: Fisher's precision parameter.

[a]Rejected from the mean calculation.

Antofagasta region, show a well-defined single vector (ChRM) direction observed during thermal demagnetization in the temperature range 150–500°C (Figure 7). Although most of the magnetization is unblocked at temperatures lower than 550°C, low values of magnetic susceptibility (Table 1) and IRM acquisition suggest that magnetite is not plentiful in these rocks. For most samples, alternating field demagnetization up to 100 mT was inefficient in removing the characteristic magnetization. Hematite is thus the likely magnetic carrier of the ChRM.

[33] The characteristic directions are well grouped in in situ coordinates and show an increase in dispersion upon tilt correction (Table 2 and Figure 7e). That magnetic polarity is normal and especially that nearby volcanics belong to the mid-Cretaceous Paradero del Desierto Formation suggest

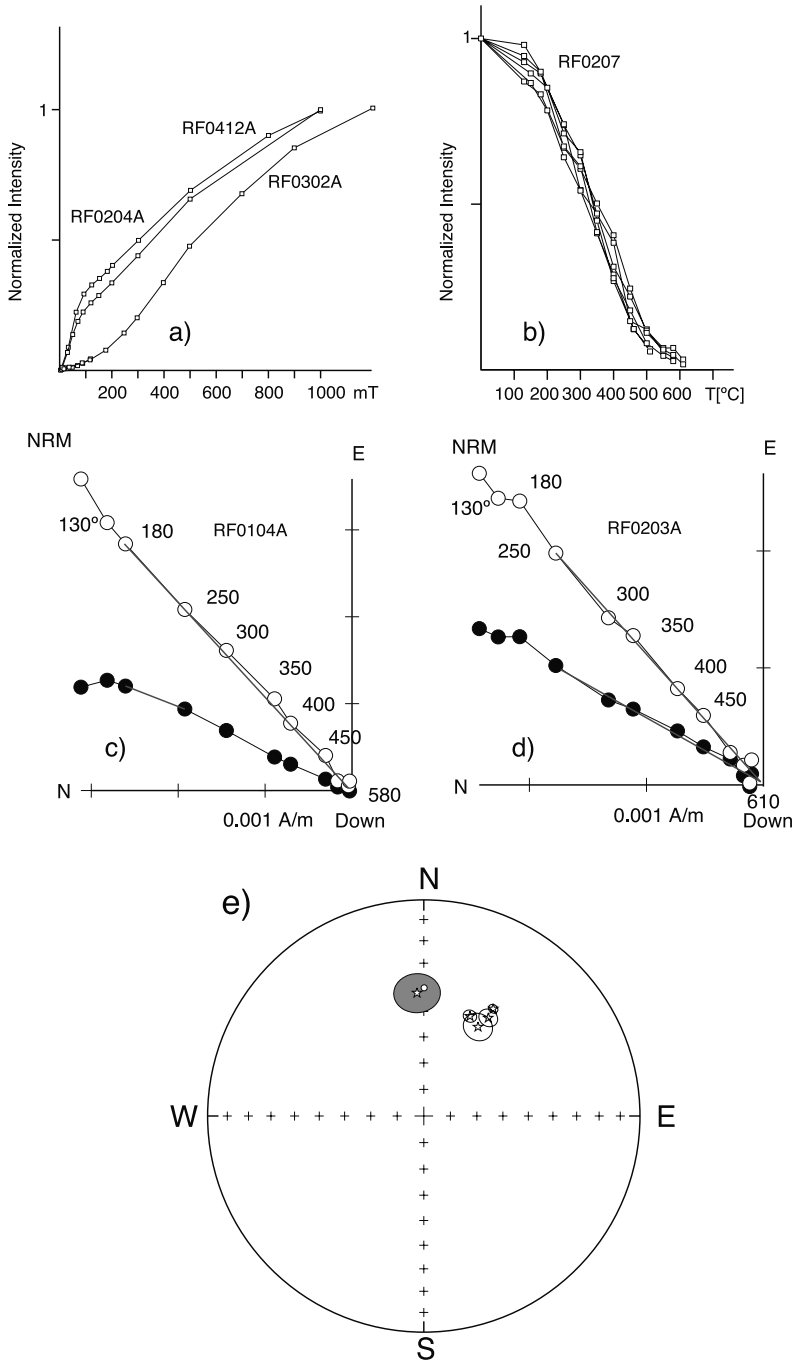

Figure 7. Magnetic properties of remagnetized Jurassic limestones. (a) Normalized isothermal remanent magnetizations (IRM) for three samples of three different sites show the existence of a high coercivity mineral. (b) Variation of the intensity of the NRM during thermal demagnetization for 6 samples of site RF02 demonstrate that the ChRM has unblocking temperatures between 150°C and 500°C. (c and d) Orthogonal projections (in situ) of thermal demagnetization diagrams. (e) Equal-area projection of site-mean characteristic directions in in-situ coordinates from Rencoret Formation (Table 2).

that remagnetization was acquired during emplacement of the Paradero del Desierto volcanics.

4.3. Paradero del Desierto Formation: Central Valley

4.3.1. Remagnetization

[34] East of Baquedano (sites PD13–PD16), a remagnetization is observed at 4 sites with different lithologies (PD13–PD16). These sites are a few hundred meters apart. In all samples a ChRM of normal polarity was observed in the temperature range 150–450°C (Figure 8). However, some samples yielded a reverse polarity component in a limited temperature range (470–610°C). In several samples, a normal polarity component of magnetization, similar to the one observed in the low unblocking temperature range, was observed above 610°C.

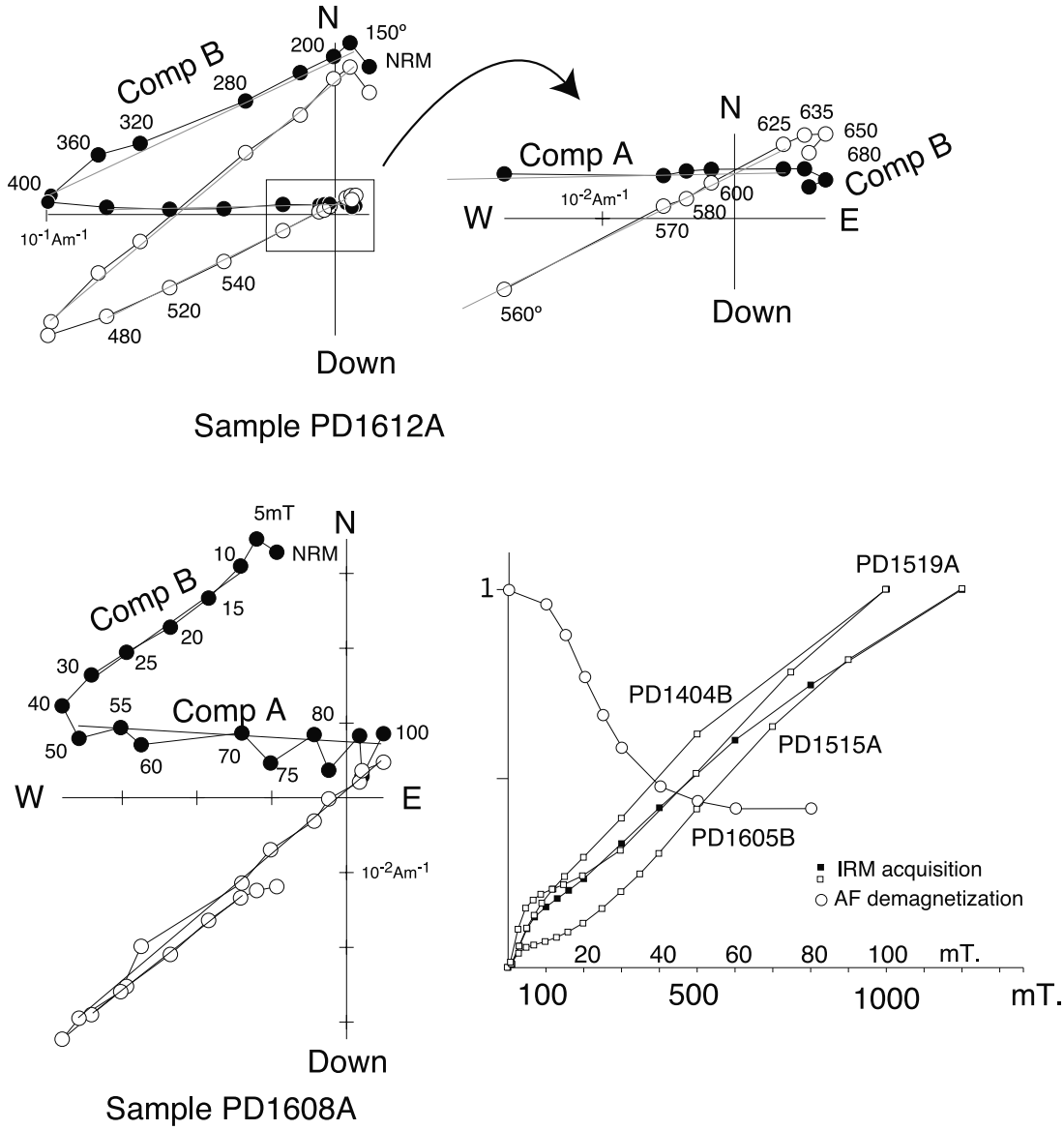

Figure 8. Orthogonal projections (tilt corrected) of thermal or AF demagnetization diagrams for remagnetized samples of Paradero del Desierto Formation. Normalized IRM acquisition and variation of intensity of the remanent magnetization during AF demagnetization (bottom right side). A normal component of magnetization (comp. B) is observed in the temperature range 150–400°C and at high temperatures above 650°C while a reverse component of magnetization (comp. A) is likely carried by magnetite.

[35] There is no evidence for low-grade metamorphism in these rocks but oxidation is widespread. Site PD14 is in lacustrine limestone with fractures filled by hematitic cement. IRM acquisition confirms the existence of hematite but the unblocking temperatures of the characteristic magnetization are widely distributed from 150°C up to 670°C.

[36] The remagnetized component with unblocking temperature higher than 620°C is carried by hematite, in agreement with the IRM acquisition curve (Figure 8). The magnetic carrier of the remagnetization in the temperature range 150–450°C is not well identified. This magnetization (150–450°C) is also partially demagnetized by AF and the carrier could be substituted stable maghemite. We did not encounter this remagnetization in the other sites sampled about 10 km further south. Thus this remagnetization is probably of local rather than regional extent. The steep inclination observed in in situ coordinates (−68° at site PD16) suggests that the remagnetization predates tilting in this area.

4.3.2. Primary Magnetizations

[37] For some sites in Cretaceous units (Paradero del Desierto Formation), a large decrease in susceptibility was observed during thermal demagnetization in the temperature range 250–350°C (Figures 9a and 9b). We attribute this behavior to the instability of maghemite during heating. In most cases, this magnetic phase does not carry a significant remanent magnetization (for example sample PD2105A in Figure 9d). The ChRM was easily recovered at higher temperatures and generally thermal demagnetization proved

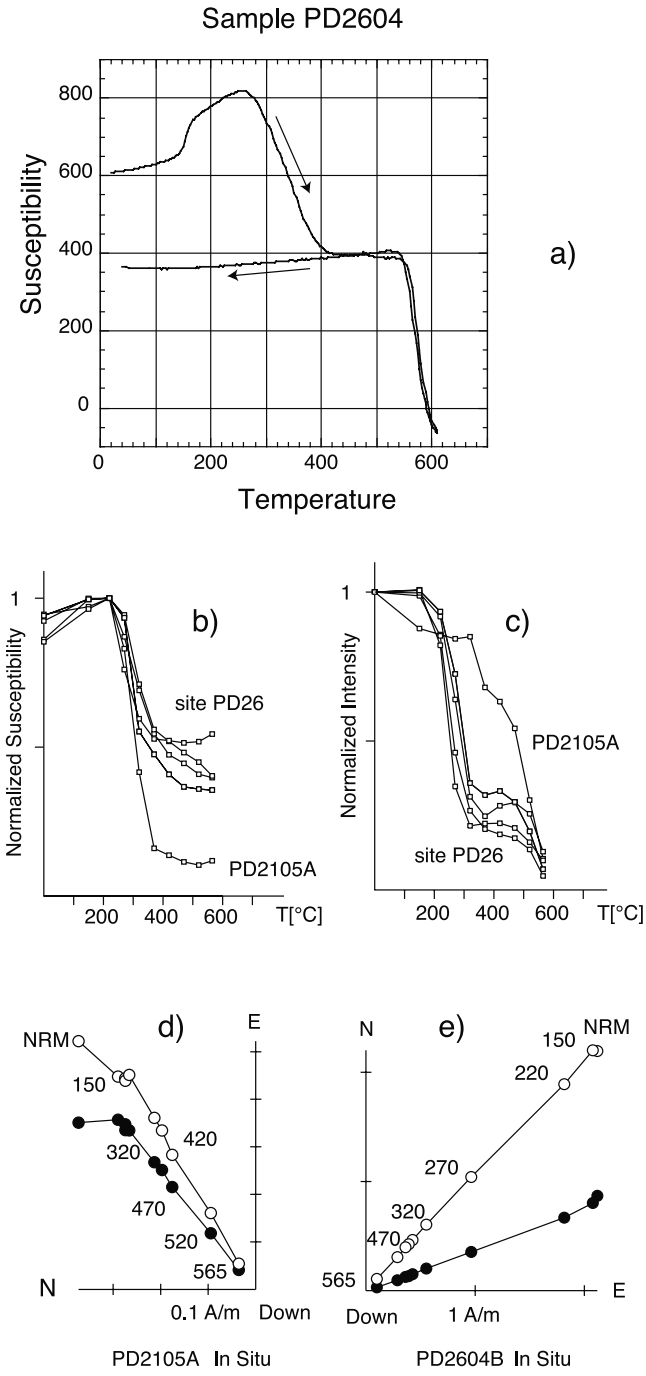

Figure 9. (a) Evidence for maghemite during K-T experiment for one sample of site PD26. During cooling, only magnetite can be identified. Measurements of magnetic susceptibility after each step of thermal demagnetization (b) demonstrate the destruction of a magnetic phase. This behavior is especially well defined for sample PD2105A in the temperature range 250–350°C. (c) The NRM is however not significantly destroyed during demagnetization below 350°C in contrast with the behavior of all samples from site PD26. (d) and (e) Orthogonal diagrams of thermal demagnetization showing well-defined univectorial ChRM.

to be more efficient in isolating ChRM than AF demagnetization. At one site (PD26), about 80% of the characteristic magnetization were unblocked at temperatures lower than 300°C (Figure 9c). Thermomagnetic experiments suggest that the low unblocking magnetic phase is maghemite. Although further magnetic studies are necessary to understand the effect of maghemitization in this site, the magnetization carried by the low temperature magnetic carrier is identical to the magnetization with unblocking temperature above 400°C. This well-defined ChRM (Figure 9e) is unambiguously different from the present-day field and is relevant to our tectonic study and likely pretectonic.

[38] At the other sites, most of the samples show univectorial (single vector) ChRM directions pointing to the

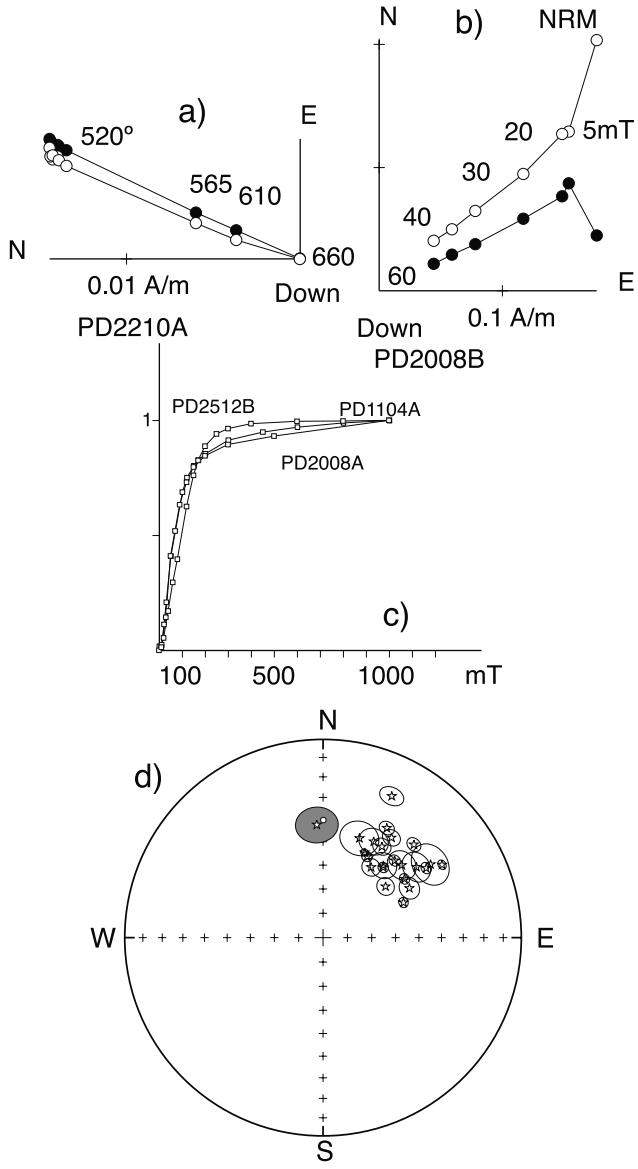

Figure 10. Orthogonal projections (in situ) of thermal (a) or AF (b) demagnetizations for samples of Paradero del Desierto Formation. (c) Normalized isothermal remanent magnetization (IRM). (d) Equal-area projection of site-mean characteristic directions in tilt corrected coordinates from Paradero del Desierto Formation. Same conventions as in Figure 6.

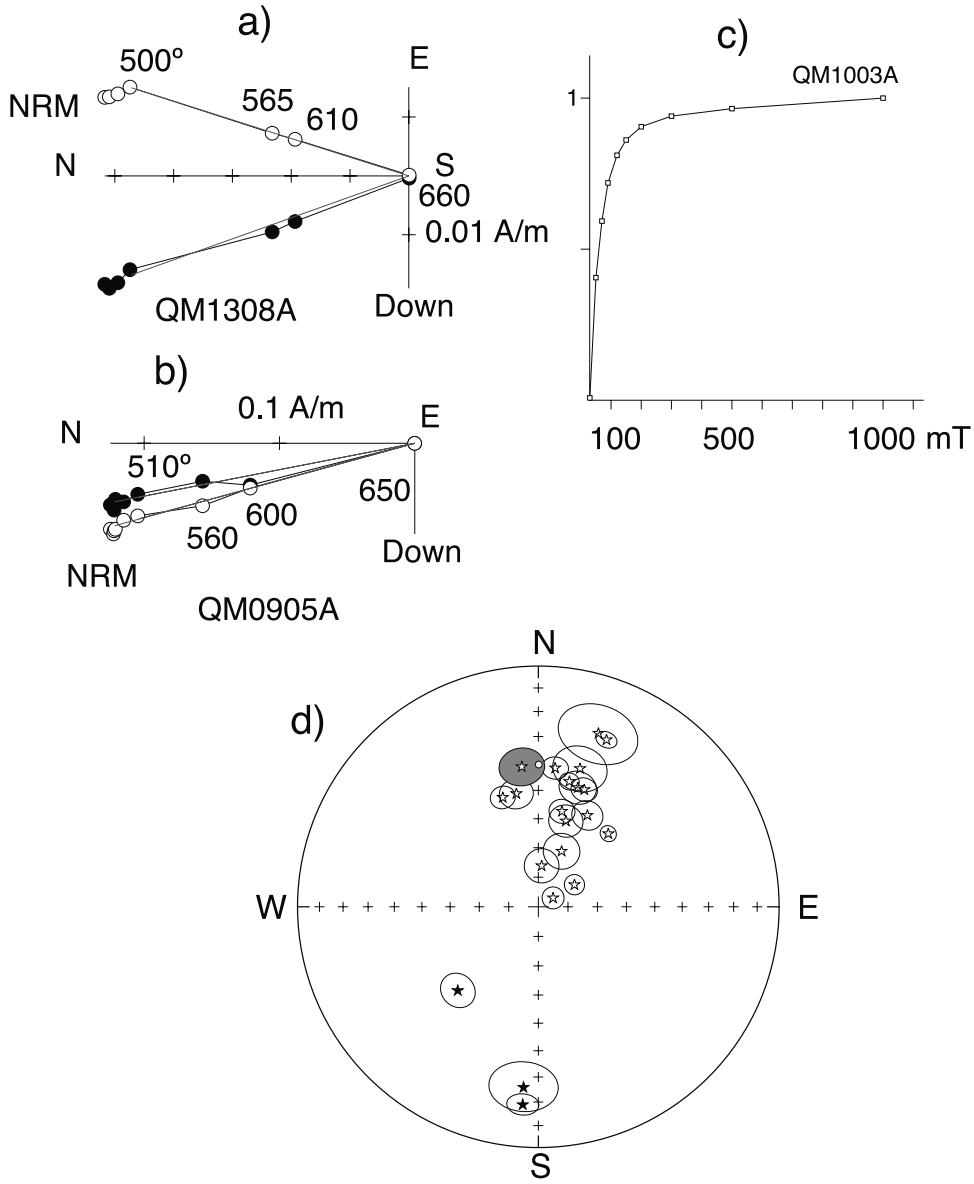

Figure 11. (a and b) Orthogonal projections (in situ) of thermal demagnetizations for samples of Quebrada Mala Formation. (c) Normalized isothermal remanent magnetization (IRM). (d) Equal-area projection of site-mean characteristic directions in tilt corrected coordinates from Quebrada Mala Formation.

origin during demagnetization (Figures 10a and 10b). Hematite and magnetite, in agreement with the IRM acquisition curve (Figures 10a and 10c) carry ChRM directions with unblocking temperatures up to 650°C.

[39] The ChRM directions were determined by least squares fit through the origin using demagnetization data in the temperature range 260–670°C.

[40] There is a slight decrease in dispersion upon tilt correction in the sites from Paradero del Desierto Formation, especially for the inclination (Figure 10d). The characteristic magnetization has a normal polarity in agreement with radiometric dating (unpublished data, SERNAGEOMIN Chile) suggesting that most of these volcanic rocks were emplaced during the long normal Cretaceous superchron.

[41] Sites (PD13–PD16) whose ChRM correspond to a remagnetization have high inclination in in situ coordinates (Table 2) and we believe that the magnetization is pretectonic. These results are included in the mean calculation for the Formation. Dispersion is relatively low (Figure 10d), especially for the inclination, supporting the hypothesis that secular variation of the geomagnetic field was lower during the Cretaceous long normal period [*McFadden et al.*, 1991; *Cronin et al.*, 2001]. The large deviations of the declinations from the expected direction provide evidence for large tectonic rotations.

4.4. Quebrada Mala Formation

[42] Most of the samples have univectorial ChRM directions (Figures 11a and 11b). Hematite and magnetite, in

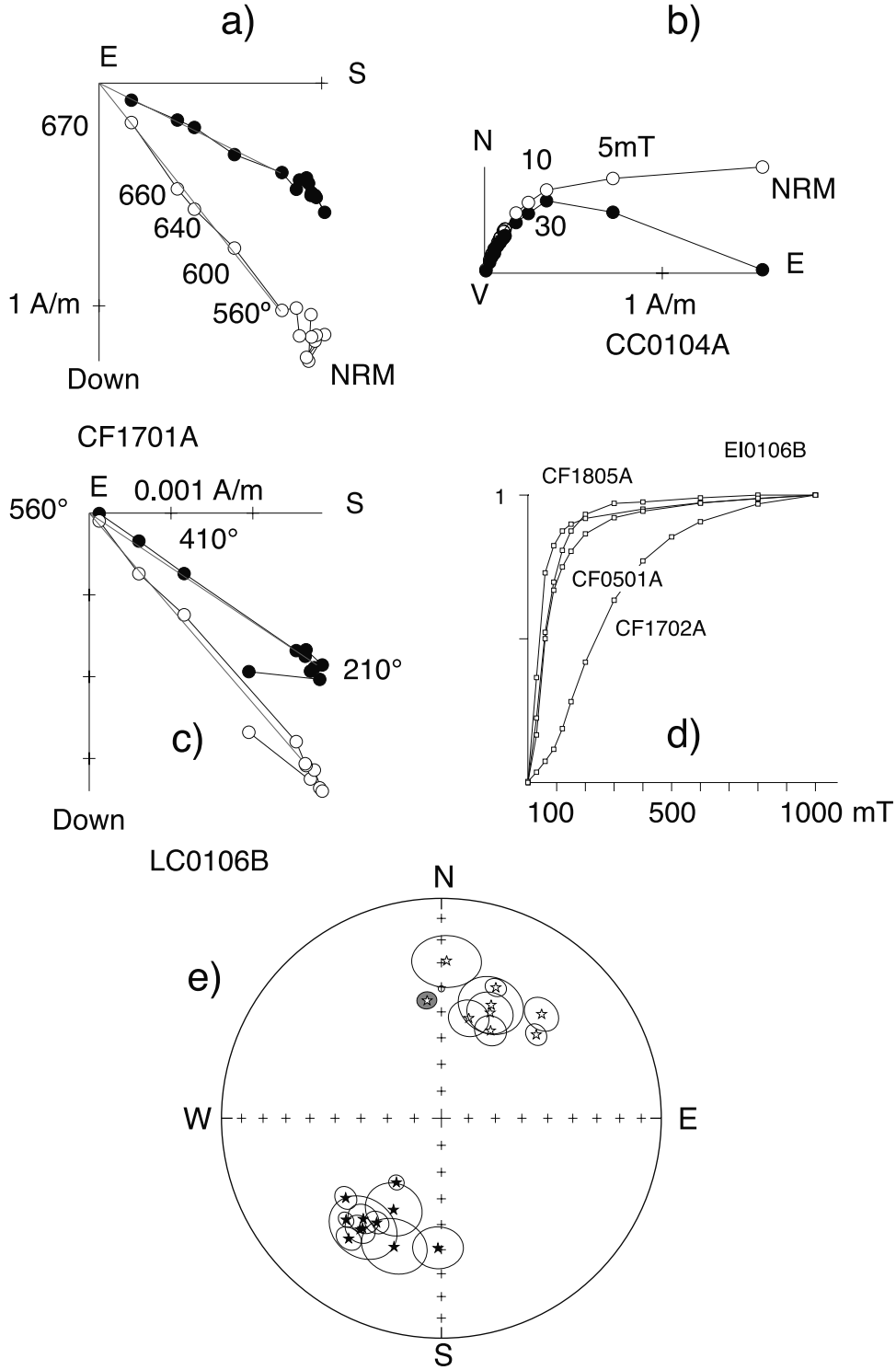

Figure 12. Paleomagnetic results in Paleogene rocks: (a–c) Orthogonal projections (in situ) of thermal or AF demagnetization. (d) Normalized isothermal remanent magnetization (IRM). (e) Equal-area projection of site-mean characteristic directions in tilt corrected coordinates.

agreement with the IRM acquisition curve (Figure 11) carry ChRM directions with unblocking temperatures up to 650°C.

[43] The ChRM directions were determined by least squares fit through the origin using demagnetization data in the temperature range 260–670°C.

[44] In most of volcanic rocks from Quebrada Mala Formation, the magnetizations are interpreted as primary, in agreement with the high dispersion of the characteristic mean-site directions in in situ coordinates (Table 2). Several sites from the Quebrada Mala Formation were taken from the Sierra del Buitre area where bedding attitude is often

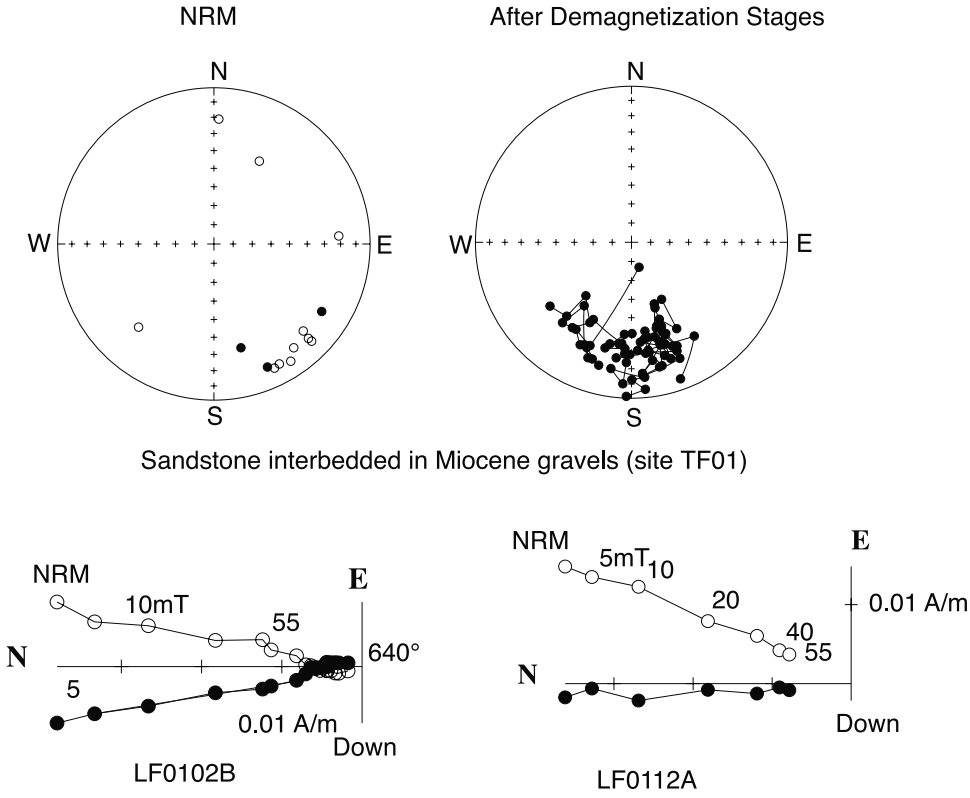

Figure 13. Top: Equal-area projection of NRM for samples of sandstone interbedded in Miocene gravels (left) and directions observed for 9 samples after each step of thermal demagnetization in the temperature range 310–640°C. Bottom: Orthogonal projections (in-situ) of thermal and AF demagnetizations for samples of the El Loa Formation. For sample LF0102B, thermal demagnetization was applied after AF demagnetization at 55 mT.

steep, in contrast with the gently folded area where we sampled the Paradero del Desierto volcanics. Sites with steep magnetic inclinations after bedding correction are in ignimbrites with steep bedding. However, the bedding attitude was determined using interbedded sediments and should not induce inclination errors. Dispersion decreases strongly upon tilt correction, giving a positive fold test (Figure 11d).

4.5. Cinchado Formation

[45] Interpretation of the demagnetization diagrams are in all cases straightforward (Figures 12a–12c). Again magnetite and hematite are the main magnetic carriers of the ChRM (Figure 12d). The reverse magnetization observed in the intrusive rock at site LC02, located nearby site CF05 where bedding dips at 60°, suggests that the intrusive rocks was not affected by the nearby deformation or postdates that deformation. In the Cinchado Formation and related intrusive rocks the observation of normal and reverse polarity magnetizations is in agreement with an Early Tertiary age for these rocks (Figure 12e). The reversal test is statistically positive. Dispersion of paleomagnetic directions decreases upon tilt correction but the fold test is inconclusive because of gentle bedding dips (Table 2 and Figure 12e). Large deviations of the observed declinations from the expected declination again are evidence for clockwise rotations.

4.6. Oligocene–Miocene Sedimentary Rocks

[46] In the Antofagasta region, it is very hard to find fine-grained upper Tertiary sediments. We have collected samples from one site (TF01) where semiconsolidated sediments are interbedded with coarse Atacama gravels (Table 1). Unfortunately, it was not possible to recognize a well-defined ChRM for this site. AF demagnetization up to 30 mT removes a secondary overprint. Thermal demagnetization following AF cleaning yields ChRM directions grouped around a reverse polarity direction (Figure 13).

[47] At the intersection of the El Loa River and the Panamericana road, we have collected 21 samples from subhorizontal, Cenozoic red siltstones of the El Loa Formation (LF01). These samples were first subjected to AF demagnetization and then to thermal demagnetization. A univectorial ChRM direction of normal polarity was observed during demagnetization up to 560°C (Figure 13).

4.7. Upper Miocene Sifón Ignimbrite

[48] Samples of the upper Miocene Sifón ignimbrite were collected at 3 sites (Table 1). The unusual positive inclination (Figure 14) recorded by the Sifón ignimbrite permits

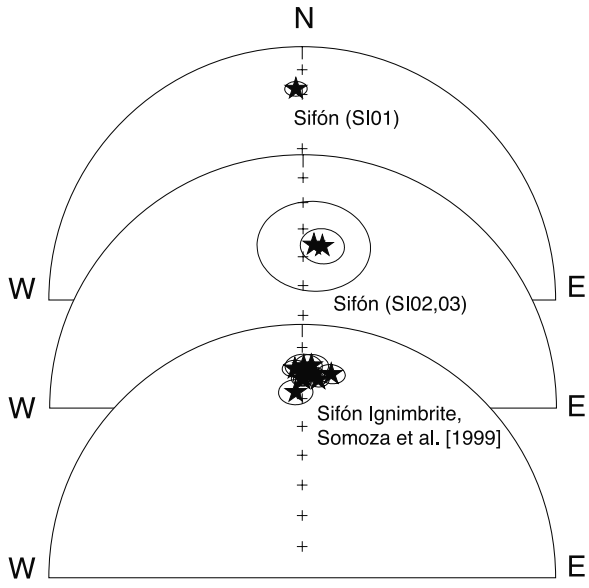

Figure 14. Equal-area projection of site-mean directions for sites of the Sifón Ignimbrite [*Somoza et al.*, 1999; this study].

straightforward paleomagnetic correlation between geographically dispersed sites. This unit is the most extensive ignimbrite in the study area of the Antofagasta region. It results from highly explosive volcanism around 8.3–8.4 Ma [*Naranjo et al.*, 1994; *Somoza et al.*, 1999; *Somoza and Tomlinson*, 2002]. Both AF and thermal demagnetization were successful in isolating a stable ChRM direction. For most of the samples the ChRM direction is univectorial. ChRM were generally demagnetized in the temperature range 210–660°C, or in the range 5–40 mT.

5. Tectonic Rotations Within the Antofagasta Region

[49] Tectonic rotations and inclination anomalies have been calculated from Mesozoic to Cenozoic units, using the estimated age of magnetization and the reference poles provided by *Besse and Courtillot* [2002]. The site-mean directions for each locality and the tectonic rotations and inclination errors are given in Table 3.

[50] Assuming that most sites in a same rock formation belong to a structural block, for which we can calculate a mean tectonic rotation (Table 3), we obtain the following results.

1. Tectonic rotations vary, from almost zero ($-2.2 \pm 13.3°$) in the coastal La Negra Volcanics, to $45.6 \pm 8.1°$ in the Paradero del Desierto volcanics.

2. There are no significant inclination errors, suggesting that changes in latitude cannot be determined paleomagnetically.

3. There is no correlation between age of rock formation and tectonic rotation.

[51] However, sites from the Paradero del Desierto and Cinchado formations show greater variations in declination than in inclination, in contrast to what is expected for the secular variation of the Earth's magnetic field at this latitude. We believe that part of the between-site dispersion is due to relative tectonic rotations. Better to understand spatial variations in tectonic rotations, 16 localities were defined (Table 3 and Figures 4, 5, and 15). Criteria used in defining the localities are (1) sites are within a homogeneous structural block and (2) the magnetization has the same age for all the sites within the locality. The number of sites characterizing the localities is variable and 5 localities out of 16 are defined with only 2 sites (Figures 4 and 5).

[52] In the locality 1 the in situ ChRM direction found at these four sites of the Rencoret Formation is similar to the tilt-corrected direction found at sites PD18 and PD19 of the Paradero del Desierto Formation located about 10 km to the NE of the remagnetized area. The mean direction for the locality corresponds to the four in situ directions in limestone sites and the other two tilt-corrected directions. The ChRM acquisition age probably reflects the mid-Cretaceous age of the Paradero del Desierto Formation. A clockwise rotation of about 32° is inferred for this locality. For localities 2, 3, and 4 the average direction, after tilt correction, shows large clockwise rotations, from about 37° up to about 50° at two localities. As in locality 1, the inclination error is small.

[53] At localities 6–9 of the Quebrada Mala Formation the rotations are not so well defined because of the higher scatter possibly induced by a poor averaging of secular variation. However, rotations are again clockwise, varying from 4.6° to 35.0°.

[54] Clockwise rotations in the localities 10–14 of the Cinchado Formation vary from 8.6° up to 53.3°. However, the smallest rotation is only defined by 2 sites at locality 13. Rotations are larger than 30° at 4 localities out of 5 within the Paleocene arc.

[55] As discussed before, in the volcanics rocks of the La Negra Formation (Localities 15 and 16) high secular variation was inferred from the paleomagnetic data. For this reason, the tectonic parameters have greater uncertainties than those observed at other localities. It is however interesting to note that both localities (Tocopilla and Antofagasta) do not show evidence for significant rotations.

6. Discussion

6.1. Timing of Rotations

[56] The Andes of northern Chile have registered several events of deformation through time since the early Mesozoic. The tectonic rotations observed in the Antofagasta region could be the result of one or several episodes of deformation.

6.1.1. Maximum Age of Rotations

[57] A close inspection of Table 3 and Figure 15 shows that whatever the magnetization age or the sequence ages, rotations in Jurassic and mid-Cretaceous sequences (Rencoret and Paradero del Desierto formations) are not systematically larger than those in Late Cretaceous–Paleocene units. This could suggest that no rotations occurred before Paleocene time. However, Cenozoic and Mesozoic units are in general not found within the same block because of the eastward shift with time of the volcanic arc. Thus we cannot reject the hypothesis that rotations observed in Cretaceous units occurred prior to the emplacement of the Cinchado Formation.

Table 3. Tectonic Rotations

Lat	Long	Decl	Inc	α95	R	ΔR	F	ΔF	Area	Age (Ma)
−22.2	−70.2	9.1	−39.2	12.0	−2.2	13.3	3.0	11.2	La Negra	180
−23.3	−69.8	30.7	−45.9	5.6	34.1	8.7	−3.5	8.4	Rencoret	100
−23.3	−69.8	42.2	−44.6	5.0	45.6	8.1	−2.2	8.1	Paradero	100
−23.2	−69.4	15.6	−51.9	9.5	22.5	13.4	−10.8	9.9	Q. Mala	80
−23.1	−69.2	29.8	−42.7	5.4	36.6	6.4	2.3	5.1	Cinchado	60
−23.6	−69.8	28.4	−45.6	4.0	31.8	7.5	−2.9	7.7	1	100
−23.5	−69.8	45.2	−44.6	10.2	48.6	12.9	−2.0	10.8	2	100
−23.3	−69.8	49.2	−39.7	6.9	52.6	9.3	2.7	9.0	3	100
−23.2	−69.6	33.3	−50.2	9.5	36.6	13.3	−7.9	10.4	4	100
−23.8	−69.6	18.8	−35.7	–	22.1	–	6.8	–	5	80
−23.5	−69.5	23.3	−57.0	–	30.2	–	−15.6	–	6	80
−23.2	−69.5	14.3	−35.9	24.1	21.2	24.8	5.2	20.3	7	80
−23.2	−69.4	357.7	−53.8	17.7	4.6	25.3	−12.7	15.5	8	80
−23.1	−69.2	28.2	−63.6	19.3	35.0	38.8	−22.7	16.7	9	80
−23.2	−69.0	46.5	−39.9	–	53.3	–	5.2	–	10	60
−23.1	−69.2	28.1	−45.0	10.5	34.9	12.2	0.0	8.9	11	60
−23.4	−69.2	34.2	−41.7	8.1	41.1	9.1	3.6	7.0	12	60
−23.2	−69.2	1.7	−34.8	–	8.6	–	10.4	–	13	60
−23.0	−69.0	34.8	−42.6	–	41.6	–	2.3	–	14	60
−22.2	−70.2	5.6	−38.3	20.4	−5.7	21.6	3.9	17.3	15	180
−23.7	−70.4	17.3	−45.9	19.9	5.9	23.9	−1.7	16.8	16	180
−23.7	−70.4	9.0	−25.0	7.0	12.4	6.5	11.4	6.2	[a]	120
−23.7	−70.4	26.0	−34.0	8.0	29.4	8.0	2.4	6.9	[b]	120
−22.7	−68.3	41.0	−36.0	9.0	47.8	10.3	4.5	9.7	[c]	80
−23.3	−69.7	53.2	−37.9	8.3	60.1	8.8	7.3	7.2	a	60
−23.3	−68.8	59.8	−35.3	14.9	66.6	–	10.0	–	b	60
−23.2	−68.6	37.0	−39.8	11.7	43.8	12.5	5.4	9.8	c	60
−23.2	−68.6	36.6	−39.0	10.6	39.9	12.4	3.3	11.0	d	100
−23.2	−68.6	15.6	−41.0	16.7	22.4	18.6	0.1	14.8	e	80
−23.1	−68.5	7.9	−46.2	20.7	14.7	25.1	−5.2	17.7	f	80
−23.0	−68.5	19.6	−38.4	10.5	22.9	12.3	3.7	11.0	g	100
−22.8	−68.2	−3.1	−43.0	12.0	3.7	14.2	−2.3	11.5	h	80
−22.8	−68.5	12.4	−37.0	15.3	19.2	16.3	3.6	13.8	i	80
−22.2	−68.2	359.9	−38.9	6.4	2.1	7.0	6.8	5.8	j	20
−22.4	−68.1	6.2	−38.0	6.7	8.7	7.6	9.1	6.5	k	30
−22.3	−68.3	31.4	−36.9	4.3	34.7	7.3	4.2	8.0	L	100
−23.4	−70.1	41.0	−44.8	7.9	43.4	10.4	−6.0	9.4	M	150

Lat–Long: Position of the localities used in the calculation of the tectonic parameters. R± ΔR, F± ΔF: rotation and flattening parameters and their associated errors [*Demarest*, 1983]. Localities 1–16 [this study]. Localities a–i [*Arriagada et al.*, 2000]. Localities j (El Loa Fm.), k (San Pedro Fm.), and L (Purilactis Fm.) [*Somoza and Tomlinson*, 2002]. Locality M: Mantos Blancos ore body [*Tassara et al.*, 2000]. Age Ma: is the reference pole used to calculate the rotation [*Besse and Courtillot*, 2002]. 20 Ma: 84.7°, 133.8°, α_{95} = 2.7; 30 Ma: 83.7°, 132.6°, α_{95} = 3.8; 60 Ma: 82.9°, 170.4°, α_{95} = 2.8; 80 Ma: 83.7°, 196.2°, α_{95} = 5.9; 100 Ma: 86.7°, 177.9°, α_{95} = 6.7; 120 Ma: 85.3°, 247.1°, α_{95} = 2.3; 150 Ma: 87.3°, 232.7°, α_{95} = 6.2; 180 Ma: 79.4°, 33.9°, α_{95} = 5.4.

[a]Coloso Area [*Tanaka et al.*, 1988].

[b]Coloso Area [*Turner et al.*, 1984].

[c]Purilactis Fm. [*Hartley et al.*, 1992].

[58] If there was only one event of rotation (for all the area), paleomagnetic results obtained in Paleocene volcanic rocks of the Cinchado Formation constrain the maximum possible age of rotation to be Paleocene. This observation is also supported by results obtained along the eastern border of the Domeyko Cordillera in Upper Cretaceous–Paleocene volcanic rocks of the Purilactis Group [*Arriagada et al.*, 2000]. Further south in the Copiapo–Vallenar area, *Gibson et al.* [2001] also found similar large clockwise rotations in Mesozoic coastal intrusives rocks and in lower Tertiary volcanic rocks. This observation suggests that most rotations along the Chilean margin could have occurred during the Early Tertiary.

6.1.2. Minimum Age of Rotation

[59] Unfortunately, most of the Oligocene and Neogene rocks within our study area are conglomerates, which are inappropriate for paleomagnetic studies. Our best result comes from Oligocene to Miocene fine-grained sediments within the Loa basin (Figure 2) where there is no evidence for clockwise rotation (Table 2). The other evidence for lack of rotation was obtained within a 2 m thick sandstone interbedded in Neogene conglomerates but this result can only be seen as tentative, because of the poor paleomagnetic data observed for that site. Our results support the hypothesis of *Somoza and Tomlinson* [2002] that the whole area did not rotate during the Neogene.

[60] Results of *Somoza et al.* [1999] come from Miocene sedimentary rocks from the Calama basin covered by the Sifón Ignimbrite. The ca. 8 Ma Sifón Ignimbrite [*Naranjo et al.*, 1994] recorded an anomalous paleomagnetic direction with a positive inclination probably associated with a polarity transition or excursion of the geomagnetic field. Paleomagnetic correlations between different sites are straightforward because this paleomagnetic direction is most probably associated with a unique volcanic event. Paleomagnetic results from several sites in the Sifón Ignimbrite within the Calama area [*Somoza et al.*, 1999] show no significant relative rotations between sites. We took 3 sites in the same Sifón Ignimbrite, two of them

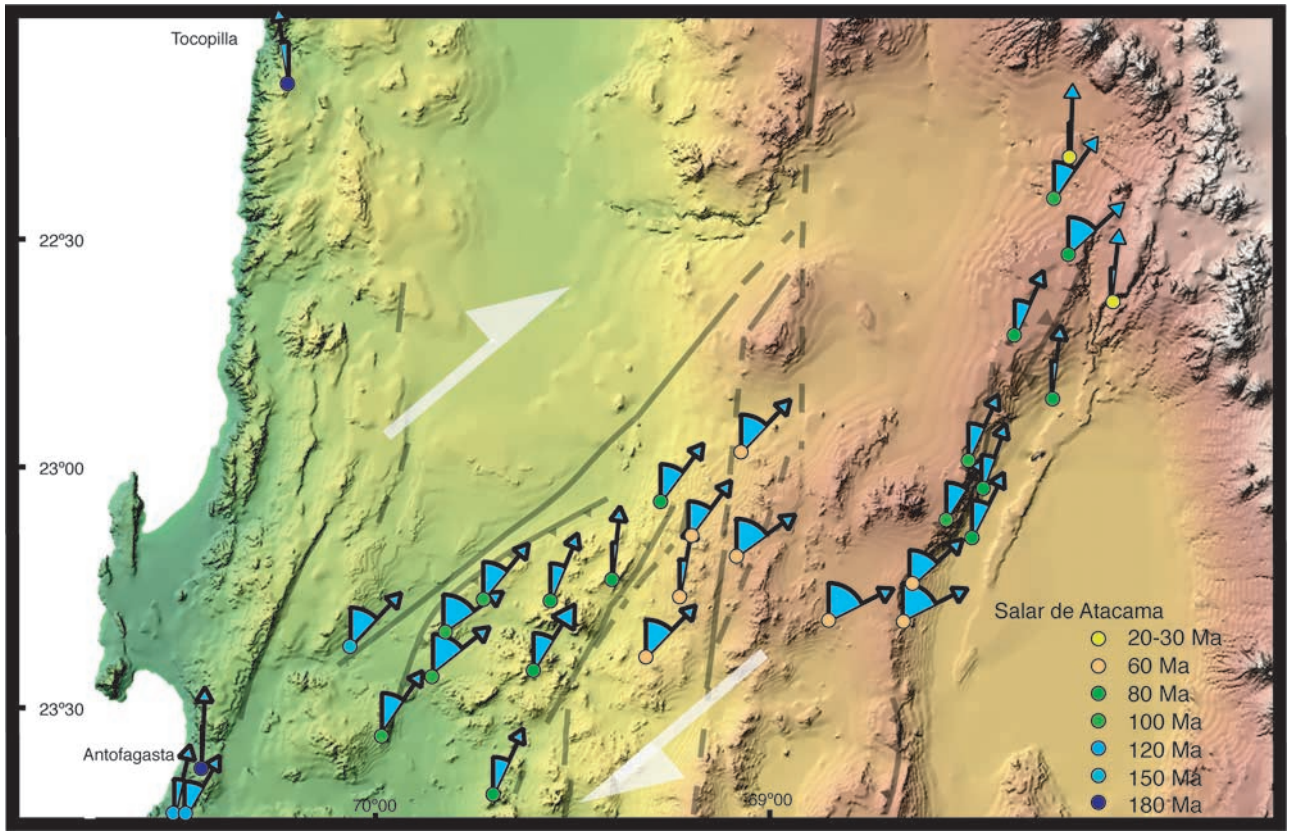

Figure 15. Tectonic rotations (deviations of arrows from a NS direction) and main structural features shown by a digital elevation model for the Antofagasta region. Colored circles are showing the age of the magnetization.

being about 50–80 km to the SW of the area sampled by *Somoza et al.* [1999]. Our results for the Sifón Ignimbrite (sites SI01–SI03, Figure 14) are very close to the direction determined by *Somoza et al.* [1999]. No internal block rotations or deformations occurred in this region of northern Chile since the emplacement of the Sifón Ignimbrite in the late Miocene.

6.2. Relation Between Tectonic Rotations and Regional Structural Pattern

[61] The mean rotation for all localities (including those previously published for the Antofagasta region listed in Table 3) in Mesozoic and Paleocene rocks is 30.8 ± 17.9°, whereas there is no inclination error (Flattening = 0.6 ± 7.6°). As discussed before, the lack of inclination error demonstrates the accuracy of the reference SA APWP used to calculate the tectonic parameters. Also, the low standard deviation associated with inclination error demonstrates that secular variation is roughly canceled at each locality, despite the small number of sites at some places. The variation in magnitude of the rotations from about 0° up to 65° with a standard deviation of about 18° around the mean is thus principally due to local tectonic effects.

[62] The variations in the amount of tectonic rotation indicate that this part of the northern Chilean Andes did not behave as a single rigid block prior to the Neogene and that there is a significant component of in situ block rotations. However, it is not easy to discard the hypothesis that there is a "hidden" component of regional rotation upon which a variable local component is superimposed.

[63] Tectonic rotations along the central Andes form a well-defined pattern of counterclockwise rotations north of the Arica elbow and clockwise rotations farther south. Several authors have suggested that the rotations may be due to oroclinal bending, associated with uplift of the Altiplano–Puna plateau [*Butler et al.*, 1995; *MacFadden et al.*, 1995]. *Coutand et al.* [1999] and *Roperch et al.* [2000] have suggested that rotations in the Altiplano–Puna plateau correlate with the trends of the main tectonic structures and occurred during the Miocene. Our results from Cenozoic semiconsolidated sediments and the Miocene Sifón Ignimbrite, are compatible with previous results from Miocene ignimbrites along the forearc [*Roperch et al.*, 2000] and from Miocene sediments from the Calama basin [*Somoza et al.*, 1999; *Somoza and Tomlinson*, 2002], which show no evidence of rotation. Therefore, any late Neogene bending leading to the development of the Bolivian orocline did not affect the forearc and the formation of the Altiplano–Puna plateau during the Neogene cannot be explained by bending of the whole margin. Instead, we believe that the forearc could have acted as a translating rigid block, which indented the Altiplano during Neogene times without rotating.

[64] A component of oroclinal bending prior to the Neogene possibly occurred in southern Peru [*Roperch and Carlier*, 1992; *Macedo Sanchez et al.*, 1992] but a bending

of the whole Chilean forearc through about 30° seems unrealistic.

[65] Although further paleomagnetic studies are required, to better define the timing and the regional extent of tectonic rotations, the results so far point to a heterogeneous pattern of rotations, where large values concentrate in small areas. This contrasts with the idea of a uniform rotation of the whole northern forearc. According to the plate convergence vectors published by *Pardo-Casas and Molnar* [1987], NNE directed convergence in northern Chile during the Eocene should result in NS dextral transpression along the margin. However, field evidence in the Cordillera de Domeyko is for left-lateral displacements during the Eocene [*Mpodozis et al.*, 1993; *Tomlinson et al.*, 1994]. To explain the strike-slip displacements opposite to the sense predicted by plate convergence models, *Arriagada et al.* [2000] suggested that distributed shear was driven by oblique convergence and that shear traction at the base of the brittle crust played a major role in driving the rotations [*Yañez et al.*, 1994; *Beck*, 1998; *Bourne et al.*, 1998].

[66] Field observations indicate that the strike-slip movements were accompanied by large E-W shortening and regional uplift leading to a rapid unroofing of the Cordillera de Domeyko [*Alpers and Brimhall*, 1988; *Maksaev and Zentilli*, 1999]. A secondary component of oblique strike-slip displacement probably existed in transfer zones, accommodating variations in the amount of EW shortening along the orogen. Within this framework, we suggest that during the Incaic event, due to differential E-W shortening, major NNE-NE shear zones developed. Structures like the ''Lineamiento Antofagasta–Calama,'' Sierra del Buitre Fault, the NNE-SSW curvature of the Atacama Fault Zone, are likely manifestations of this event (see Figures 2, 4, 5, and 15). There is no direct evidence that the postulated major structure ''Lineamiento Antofagasta–Calama'' along the main road between Antofagasta and Calama corresponds to a major dextral shear zone. However, gravity data [*Götze and the Migra Group*, 1996] suggest that the eastern border of the Coastal Cordillera is significantly displaced to the east, north of the ''Lineamiento Antofagasta–Calama.'' We can also observe that the axis of the Cretaceous magmatic arc is also shifted toward the east near Calama. Dextral transpression along the ''Lineamiento Antofagasta–Calama'' could explain the apparent difference in the location of the Mesozoic units north and south of this NE oriented structure and the widespread occurrence of large clockwise rotations. Our interpretation will require checking by means of detailed structural studies, notably of fault displacements and their timing.

7. Conclusions

[67] We have obtained satisfactory paleomagnetic results from a study of 108 sites from sediments, volcanics and intrusive rock of Mesozoic to Cenozoic age, in the forearc of the central Andes in northern Chile.

[68] The average paleomagnetic inclination recorded by upper Mesozoic and lower Tertiary volcanic rocks from the study area are in good agreement with the expected inclination determined from the BC01 APWP. These results indicate that changes in latitude along the Andean forearc are not significant enough to be determined by paleomagnetic techniques. The lack of inclination errors in volcanic rocks and remagnetized sediments contrasts with the large inclination shallowing observed in upper Tertiary red beds from the Altiplano and the Puna [*Coutand et al.*, 1999; *Roperch et al.*, 1999, 2000]. Paleomagnetic results from the Andes, where relative latitudinal displacements are small, demonstrate that inclination shallowing in red beds is strong and was acquired during deposition and further compaction.

[69] Vertical axis rotations, calculated from paleomagnetic declinations, are clockwise and up to 65° in the Antofagasta region. Although the age of the rotations in this area is difficult to constrain accurately, available stratigraphic, radiometric and structural data suggest that deformation and rotations occurred during the Paleogene and probably during the Incaic orogenic event. No evidence for Neogene tectonic rotation can be found in the Chilean forearc (in the study area) suggesting that the development of the Bolivian orocline during the late Neogene and the formation of the Altiplano–Puna plateau cannot be explained by simple bending of the whole margin. We believe that the forearc acted as a translating rigid block during Neogene development of the Altiplano–Puna plateau.

[70] Traditionally, structural studies in the forearc of northern Chile have emphasized motions along major N-S fault systems (i.e., the AFS and the DFS), along which deformation is assumed to be localized. A major result of our paleomagnetic study is that widespread tectonic rotations are not closely related to these faults. Instead Paleogene deformation is much more distributed across the forearc than it was previously thought. Most fold axes and thrusts are not oriented N-S but are significantly trending to the NE (for example, Sierra del Buitre fault, Los Toros fault). We speculate that these structures are indeed rotated.

[71] Large rotations are found not only in our study area but widely spread along the Andean margin. They are clockwise along the Ecuadorian margin [*Roperch et al.*, 1987], the northern Peruvian Andes [*Mourier et al.*, 1988; *Mitouard et al.*, 1992], the Chilean forearc [*Riley et al.*, 1993; *Randall and Taylor*, 1996; *Randall et al.*, 2001; this study] and counterclockwise in central Peru and southern Peru [*Roperch and Carlier*, 1992; *Macedo Sanchez et al.*, 1992]. Tectonic rotations are indeed one of the principal structural characteristics of the Early Tertiary evolution of the Andes.

[72] **Acknowledgments.** The Institut de Recherche pour le Développement (IRD) and CONICYT (FONDECYT projects 1970002 and 199009 and student scholarship to the first author) funded most of this work. The authors thank Mathilde Basso, Pierre Gautier, Nicolas Marinovic, Andres Tassara, and Andy Tomlinson for discussions about the structural evolution of the forearc. Sampling of the La Negra Volcanics was done with the help of Gabriel Carlier and Martine Gérard. Andres Tassara and Luisa Pinto participated in one field trip and in laboratory data acquisition. Part of the paleomagnetic data processing was performed with the excellent ''Paleomac'' software written by Jean-Pascal Cogné. We thank Randall D. Forsythe and Ruben Somoza for constructive reviews.

References

Alpers, C. N., and G. H. Brimhall, Middle Miocene climatic change in the Atacama Desert, northern Chile: Evidence from supergene mineralization at La Escondida with Suppl. Data 88-21, *Geol. Soc. Am. Bull.*, *100*(3), 1640–1656, 1988.

Arriagada, C., P. Roperch, and C. Mpodozis, Clockwise block rotations along the eastern border of the Cordillera de Domeyko, Northern Chile (22°45′–23°30′S), *Tectonophysics*, *326*, 153–171, 2000.

Aubry, L., P. Roperch, M. de Urreiztieta, E. Rosello, and A. Chauvin, Paleomagnetic study along the southeastern edge of the Altiplano–Puna Plateau: Neogene tectonic rotations, *J. Geophys. Res.*, *101*, 17,883–17,899, 1996.

Beck, M. E., Jr., Tectonic rotations on the leading edge of South America: The Bolivian orocline revisited, *Geology*, *15*, 806–808, 1987.

Beck, M. E., Jr., Analysis of Late Jurassic–Recent paleomagnetic data from active plate margins of South America, *J. S. Am. Earth Sci.*, *1*, 39–52, 1988.

Beck, M. E., Jr., On the mechanism of crustal block rotations in the central Andes, *Tectonophysics*, *299*, 75–92, 1998.

Beck, M. E., Jr., Jurassic and Cretaceous apparent polar wander relative to South America: Some tectonic implications, *J. Geophys. Res.*, *104*, 5063–5067, 1999.

Besse, J., and V. Courtillot, Revised and synthetic apparent polar wander paths of the African, Eurasian, North American and Indian plates, and true polar wander since 200 Ma, *J. Geophys. Res.*, *96*, 4029–4050, 1991.

Besse, J., and V. Courtillot, Apparent and true polar wander and the geometry of the Geomagnetic Field in the last 200 million years, *J. Geophys. Res.*, *107*(B11), 2300, doi:10.1029/2000JB000050, 2002.

Boric, R., F. Diaz, and V. Maksaev, Geologia y yacimientos metaliferos de la region de Antofogasta, *Bol. Inst. Invest. Geol. Chile*, *40*(246), 2, 1990.

Bourne, S. J., P. C. England, and B. Parsons, The motion of crustal blocks driven by flow of the lower lithosphere and implications for slip rates of continental strike-slip faults, *Nature*, *391*, 655–659, 1998.

Butler, R. F., D. R. Richards, T. Sempere, and L. G. Marshall, Paleomagnetic determinations of vertical-axis tectonic rotations from Late Cretaceous and Paleocene strata of Bolivia, *Geology*, *23*, 799–802, 1995.

Carey, S. W., A tectonic approach to continental drift, in *Continental Drift: A Symposium*, edited by S. W. Carey, pp. 177–355, Geol. Dep., Univ. of Tasmania, Hobart, 1958.

Charrier, R., and K.-J. Reutter, The Purilactis Group of Northern Chile: Boundary between arc and backarc from Late Cretaceous to Eocene, in *Tectonics of the Southern Central Andes*, edited by K.-J. Reutter et al., pp. 189–201, Springer-Verlag, New York, 1994.

Coira, B., J. Davidson, C. Mpodozis, and V. A. Ramos, Tectonic and magmatic evolution of the Andes of northern Argentina and Chile, *Earth Sci. Rev.*, *18*, 303–332, 1982.

Cornejo, P., R. Tosdal, C. Mpodozis, A. J. Tomlinson, and O. Rivera, El Salvador porphyry copper revisited: Geologic and geochronologic framework, *Int. Geol. Rev.*, *39*, 22–54, 1997.

Cortés, J., *Hoja Palestina, Región de Antofagasta*, Serv. Nac. Geol. Min., Santiago, 2000.

Coutand, I., P. Roperch, A. Chauvin, P. R. Cobbold, and P. Gautier, Vertical axis rotations across the Puna plateau (northwestern Argentina) from paleomagnetic analysis of Cretaceous and Cenozoic rocks, *J. Geophys. Res.*, *104*, 22,965–22,984, 1999.

Cronin, M., L. Tauxe, C. Constable, P. Selkin, and T. Pick, Noise in the quiet zone, *Earth Planet. Sci. Lett.*, *190*, 13–30, 2001.

Demarest, H. H., Error analysis for the determination of tectonic rotation from paleomagnetic data, *J. Geophys. Res.*, *88*, 4321–4328, 1983.

Dilles, J. H., A. J. Tomlinson, M. Martin, and N. Blanco, El Abra and Fortuna Complexes: A porphyry copper batholith sinistrally displaced by the Falla Oeste, in *VIII Congr. Geológico Chileno, Antofagasta*, vol. 3, pp. 1883–1887, 1997.

Ernesto, M., I. G. Pacca, F. Y. Hiodo, and A. J. R. Nardy, Palaeomagnetism of the Mesozoic Serra Geral Formation, southern Brazil, *Phys. Earth Planet. Inter.*, *64*, 153–175, 1990.

Forsythe, R., and L. Chisholm, Paleomagnetic and structural constraints on rotations in the north Chilean coast ranges, *J. S. Am. Earth Sci.*, *7*, 279–294, 1994.

Gibson, M., G. K. Taylor, and J. Grocott, New paleomagnetic results and Ar–Ar geochronology from the Vallenar Region (29°S), N. Chile: Implications for the timing of rotations in the Andean forearc region, *Eos. Trans. AGU*, *82*(47), Fall Meet. Suppl., 2001.

Götze, H.-J., and the Migra Group, Group updates the gravity data base in the central Andes (20–29°S), *EOS Trans. AGU*, 1996. (Available as http://www.agu.org/eos_elec/95189e.html).

Grier, M. E., J. A. Salfity, and R. W. Allmendinger, Andean reactivation of the Cretaceous Salta rift, northwestern Argentina, *J. S. Am. Earth Sci.*, *4*, 351–372, 1991.

Grocott, J., M. Brown, R. D. Dallmeyer, G. K. Taylor, and P. I. Treloar, Mechanisms of continental growth in extensional arcs: An example from the Andean plate-boundary zone, *Geol. Boulder*, *22*, 391–394, 1994.

Hartley, A. J., E. J. Jolley, and P. Turner, Paleomagnetic evidence for rotation in the Precordillera of northern Chile: Structural constraints and implications for the evolution of the Andean forearc: Andean geodynamics, *Tectonophysics*, *205*, 49–64, 1992.

Heki, K., Y. Hamano, H. Kinoshita, A. Taira, and M. Kono, Paleomagnetic study of Cretaceous rocks of Peru, South America: Evidence for rotations of the Andes, *Tectonophysics*, *108*, 267–281, 1984.

Heki, K., Y. Hamano, M. Kono, and U. Tadahide, Palaeomagnetism of Neogene Ocros dyke swarm, the Peruvian Andes: Implication for the Bolivian orocline, *Geophys. J. R. Astron. Soc.*, *80*, 527–534, 1985.

Hervé, M., Movimiento sinistral en el Cretácico Inferior de la Zona de Falla de Atacama, Chile, *Rev. Geol. Chile*, *31*, 37–42, 1987.

Isacks, B. L., Uplift of the central Andean Plateau and bending of the Bolivian orocline, *J. Geophys. Res.*, *93*, 3211–3231, 1988.

Kirschvink, J. L., The least-squares line and plane and the analysis of paleomagnetic data, *Geophys. J. R. Astron. Soc.*, *62*, 699–718, 1980.

Lamb, S. H., and D. E. Randall, Deriving palaeomagnetic poles from independently assessed inclination and declination data: Implications for South American poles since 120 Ma, *Geophys. J. Int.*, *146*, 349–370, 2001.

Macedo Sanchez, O., J. Surmont, C. Kissel, and C. Laj, New temporal constraints on the rotation of the Peruvian central Andes obtained from paleomagnetism, *Geophys. Res. Lett.*, *19*(1), 1875–1878, 1992.

MacFadden, B. J., F. Anaya, and C. C. Swisher III, Neogene paleomagnetism and oroclinal bending of the central Andes of Bolivia, *J. Geophys. Res.*, *100*, 8153–8167, 1995.

Maksaev, V., and M. Zentilli, Fission track thermochronology of the Domeyko Cordillera, northern Chile: Implications for Andean tectonics and porphyry copper metallogenesis, *Explor. Min. Geol.*, *8*, 65–89, 1999.

Marinovic, N., and M. García, *Hoja Pampa Unión, Región de Antofagasta*, Serv. Nac. Geol. Min., Santiago, 1999.

May, S. R., and R. F. Butler, Paleomagnetism of the Puente Piedra Formation, central Peru, *Earth Planet. Sci. Lett.*, *72*, 205–218, 1985.

McFadden, P. L., and M. W. McElhinny, The combined analysis of remagnetization circles and direct observations in paleomagnetism, *Earth Planet. Sci. Lett.*, *87*, 161–172, 1988.

McFadden, P. L., R. T. Merrill, M. W. McElhinny, and S. Lee, Reversals of the Earth's magnetic field and temporal variations of the dynamo families, *J. Geophys. Res.*, *96*, 3923–3933, 1991.

Mitouard, P., C. Laj, T. Mourier, and C. Kissel, Paleomagnetic study of an arcuate fold belt developed on a marginal orogen: The Cajamarca deflection, northern Peru, *Earth Planet. Sci. Lett.*, *112*, 41–52, 1992.

Mourier, T., C. Laj, F. Mégard, P. Roperch, P. Mitouard, and F. Medrano, An accreted continental terrane in northwestern Peru, *Earth Planet. Sci. Lett.*, *88*, 182–192, 1988.

Mpodozis, C., and V. A. Ramos, The Andes of Chile and Argentina, in *Geology of the Andes and Its Relation to Hydrocarbon and Mineral Resources*, edited by G. E. Ericksen et al., pp. 59–90, Circum-Pac. Counc. for Energy and Min. Resour., Houston, Tex., 1990.

Mpodozis, C., N. Marinovic, and I. Smoje, Eocene left lateral strike slip faulting and clockwise block rotations in the Cordillera de Domeyko, west of Salar de Atacama, northern Chile, in *Second ISAG, Oxford, UK*, pp. 225–228, 1993.

Naranjo, J. A., C. F. Ramírez, and R. Paskoff, Morphostratigraphic evolution of the northwestern margin of the Salar de Atacama basin (23°S–68°W), *Rev. Geol. Chile*, *21*, 91–103, 1994.

Pardo-Casas, F., and P. Molnar, Relative motion of the Nazca (Farallon) and South American plates since Late Cretaceous time, *Tectonics*, *6*, 233–248, 1987.

Randall, D. E., and G. K. Taylor, Major crustal rotations in the Andean margin: Paleomagnetic results from the coastal Cordillera of northern Chile, *J. Geophys. Res.*, *101*, 15,783–15,798, 1996.

Randall, D., A. Tomlinson, and G. Taylor, Paleomagnetically defined rotations from the Precordillera of northern Chile: Evidence of localized in situ fault-controlled rotations, *Tectonics*, *20*, 235–254, 2001.

Raposo, M. I. B., and M. Ernesto, An Early Cretaceous paleomagnetic pole from Ponta Grossa dikes (Brazil): Implications for the South American Mesozoic apparent polar wander path, *J. Geophys. Res.*, *100*, 20,095–20,110, 1995.

Reutter, K. J., and E. Scheuber, Relation between tectonics and magmatism in the Andes of northern Chile and adjacent areas between 21° and 25° S, in *I Congr. Geol. Chileno*, vol. 1, pp. 345–363, Dept. de Geol. y Geofisica Univ. de Chile, 1988.

Reutter, K.-J., E. Scheuber, and G. Chong, The Precordilleran fault system of Chuquicamata, northern Chile: Evidence for reversals along arc parallel strike-slip faults, *Tectonophysics*, *259*, 213–228, 1996.

Riley, P. D., M. E. J. Beck, R. F. Burmester, C. Mpodozis, and A. García, Paleomagnetic evidence of vertical axis block rotations from the Mesozoic of northern Chile, *J. Geophys. Res.*, *98*, 8321–8333, 1993.

Roperch, P., F. Megard, L. A. J. Carlo, T. Mourier, T. M. Clube, and C. Noblet, Rotated oceanic blocks in western Ecuador, *Geophys. Res. Lett.*, *14*(1), 558–561, 1987.

Roperch, P., and G. Carlier, Paleomagnetism of Mesozoic rocks from the central Andes of southern Peru: Importance of rotations in the develop-

ment of the Bolivian orocline, *J. Geophys. Res.*, *97*, 17,233–17,249, 1992.

Roperch, P., G. Herail, and M. Fornari, Magnetostratigraphy of the Miocene Corque basin, Bolivia: Implications for the geodynamic evolution of the Altiplano during the late Tertiary, *J. Geophys. Res.*, *104*, 20,415–20,429, 1999.

Roperch, P., M. Fornari, G. Hérail, and G. Parraguez, Tectonic rotations within the Bolivian Altiplano: Implications for the geodynamic evolution of the central Andes during the late Tertiary, *J. Geophys. Res.*, *105*, 795–820, 2000.

Scheuber, E., and P. A. M. Andriessen, The kinematic and geodynamic significance of the Atacama fault zone, northern Chile, *J. Struct. Geol.*, *12*, 243–257, 1990.

Scheuber, E., and G. González, Tectonics of the Jurassic–Early Cretaceous magmatic arc of the north Chilean Coastal Cordillera (22°–26°S): A story of crustal deformation along a convergent plate boundary, *Tectonics*, *18*, 895–910, 1999.

Somoza, R., S. Singer, and A. Tomlinson, Paleomagnetic study of upper Miocene rocks from northern Chile: Implications for the origin of late Miocene–Recent tectonic rotations in the southern central Andes, *J. Geophys. Res.*, *104*, 22,923–22,936, 1999.

Somoza, R., and A. Tomlinson, Paleomagnetism in the Precordillera of northern Chile (22°30′S): implications for the history of tectonic rotations in the Central Andes, *Earth Planet. Sci. Lett.*, *94*, 369–381, 2002.

Tanaka, H., H. Tsunakawa, and K. Amano, Palaeomagnetism of the cretaceous El Way and Coloso Formations from the northern Chilean Andes, *Geophys. J. R. Astron. Soc.*, *95*, 195–203, 1988.

Tassara, A., P. Roperch, and A. Pavez, Paleomagnetismo de los yacimientos Mantos Blancos y Manto Verde: Implicancias tectonicas y cronologicas, in *IX Congr. Geol. Chileno, Puerto Varas*, vol. 2, pp. 166–170, 2000.

Tomlinson, A., C. Mpodozis, P. Cornejo, C. F. Ramírez, and T. Dumitri, El sistema de Fallas Sierra de Castillo-Agua Amarga: Transpresión sinistral eocena en la precordillera de Potrerillos–El Salvador, in *VII Congr. Geol. Chileno, Concepción*, vol. II, pp. 1459–1463, 1994.

Tomlinson, A., and N. Blanco, Structural evolution and displacement history of the West Fault System, Precordillera, Chile, part 1, Synmineral history, in *VIII Congr. Geol. Chileno, Antofagasta*, vol. 3, pp. 1873–1877, 1997a.

Tomlinson, A., and N. Blanco, Structural evolution and displacement history of the West Fault System, Precordillera, Chile, part 2, Postmineral history, in *VIII Congr. Geol. Chileno, Antofagasta*, vol. 3, pp. 1878–1882, 1997b.

Turner, P., H. Clemmey, and S. Flint, Paleomagnetic studies of a Cretaceous molasses sequence in the central Andes (Coloso Formation, northern Chile), *J. Geol. Soc. London*, *141*, 869–876, 1984.

Yañez, G., C. Mpodozis, A. Tomlinson, Eocene dextral oblique convergence and sinistral shear along the Domeyko fault system: A thin viscous sheet approach with asthenospheric drag at the base of the crust, in *VII Congr. Geol. Chileno*, vol. 2, pp. 1478–1482, 1994.

C. Arriagada and P. Roperch, Departamento de Geología, IRD, Universidad de Chile, Santiago, Chile. (cearriag@cec.uchile.cl)

A. Chauvin and P. R. Cobbold, UMR 6118 du CNRS, Géosciences-Rennes, F-35042 Rennes, France.

J. Cortés, Servicio Nacional de Geología y Minería, Santiago, Chile.

G. Dupont-Nivet, Department of Geosciences, University of Arizona, Tucson, AZ 85721, USA.

C. Mpodozis, SIPETROL, Santiago, Chile.